The Astrophysical Journal, 665:1038–1056, 2007 August 20

RADIATIVE FEEDBACK FROM MASSIVE BLACK HOLES IN ELLIPTICAL GALAXIES: AGN FLARING AND CENTRAL STARBURST FUELED BY RECYCLED GAS

Luca Ciotti[1] and Jeremiah P. Ostriker[2,3]
Received 2007 March 2; accepted 2007 May 14

ABSTRACT

We show how the observed AGN radiative output from massive black holes at the centers of elliptical galaxies affects the hot ISM of these systems with the aid of a high-resolution hydrodynamical code, where the cooling and heating functions include photoionization plus Compton heating. Radiative heating is a key factor in the self-regulated coevolution of massive BHs and their host galaxies, and (1) the mass accumulated by the central BH is limited by feedback to the range observed today and (2) relaxation instabilities occur so that duty cycles are small enough ($\lesssim$0.03) to account for the very small fraction of massive ellipticals observed to be in the "on" QSO phase, when the accretion luminosity approaches the Eddington luminosity. The duty cycle of the hot bubbles inflated at the galactic center during major accretion episodes is of the order of $\gtrsim$0.1–0.4. Major accretion episodes caused by cooling flows in the recycled gas produced by normal stellar evolution trigger nuclear starbursts coincident with AGN flaring. Overall, in the bursting phase ($1 \lesssim z \lesssim 3$), the duty cycle of the BH in its "on" phase is of the order of percents and is unobscured approximately one-third of the time, the obscuration occurring during dusty starbursts. Roughly half of the recycled gas from dying stars is ejected as galactic winds, half is consumed in central starbursts, and less than 1% is accreted onto the central BH. Mechanical energy output from nonrelativistic gas winds integrates to 2.3×10^{59} ergs, with most of it caused by broad-line AGN outflows. We predict the typical properties of the very metal-rich poststarburst central regions and show that the resulting surface density profiles are well described by Sérsic profiles.

Subject headings: accretion, accretion disks — black hole physics — galaxies: active — galaxies: nuclei — galaxies: starburst — quasars: general

1. INTRODUCTION

Supermassive black holes (SMBHs) at the centers of bulges and elliptical galaxies have played an important role in the processes of galactic formation and evolution (see, e.g., Silk & Rees 1998; Fabian 1999; Burkert & Silk 2001; Cavaliere & Vittorini 2002; King 2003; Wyithe & Loeb 2003; Haiman et al. 2004; Granato et al. 2004; Sazonov et al. 2005; Murray et al. 2005; Di Matteo et al. 2005; Begelman & Nath 2005; Hopkins et al. 2006a; Croton et al. 2006), as strongly supported by the remarkable correlations found between host galaxy properties and the masses of their SMBHs (see, e.g., Magorrian et al. 1998; Ferrarese & Merritt 2000; Gebhardt et al. 2000; Yu & Tremaine 2002; McLure & Dunlop 2002; Graham et al. 2003).

An additional very severe issue that active galactic nucleus (AGN) feedback likely addresses is that of the "cooling flow problem" (e.g., Xu et al. 2002; Peterson & Fabian 2006), which in elliptical galaxies is at least as serious as the heavily analyzed cooling flow problem in clusters (because the radiative cooling times are an order of magnitude shorter, $\sim 10^{7.5}$ yr vs. $\sim 10^{9}$ yr). Also, a rarely discussed problem is that the recycled gas (primarily from red giant winds and planetary nebulae) of the evolving stellar population expected to accumulate within galaxies over cosmic time, and responsible for the cooling flow, is orders of magnitude larger than the mass of either the central SMBH or the resident diffuse gas. Quantitatively, the mass return rate from evolving stars in elliptical galaxies can be estimated as

$$\dot{M}_*(t) \simeq 1.5 \times \frac{L_B}{10^{11}\ L_{B\odot}}\, t_{15}^{-1.3}\ M_\odot\ \mathrm{yr}^{-1}, \qquad (1)$$

where L_B is the present galactic blue luminosity and t_{15} is time in 15 Gyr units (Ciotti et al. 1991, hereafter C91; see also § 2.2). Thus, the total mass return would accumulate onto the central SMBH a mass by far too large compared with the observed SMBH masses if a long-lived cooling flow occurred. Young stellar populations observed in the body of ellipticals also cannot account for the total mass released, and alternative forms of cold mass disposal (such as distributed mass dropout/star formation) are not viable solutions (e.g., Binney 2001). In addition to this mass disposal problem, also the X-ray luminosity L_X of low-redshift elliptical galaxies is inconsistent with the standard cooling flow model. In fact, low-redshift elliptical galaxies with optical luminosity $L_B \gtrsim 3 \times 10^{10}\ L_\odot$ show a significant range in the ratio of gas to total mass at fixed L_B, with tabulated values ranging from virtually zero up to a few percent (e.g., Roberts et al. 1991), and most of that is seen in X-rays with temperatures close to the virial temperatures of the systems ($\sim 10^{6.7}$ K; e.g., O'Sullivan et al. 2003).

A (partial) solution to these problems was proposed by D'Ercole et al. (1989) and C91, by considering the effect of Type Ia supernova (SN Ia) heating of the galactic gas and exploring the time evolution of gas flows by using hydrodynamical numerical simulations. Subsequent, more realistic galactic models (with updated rates of SNe Ia derived by direct counts from optical observations) were explored by Pellegrini & Ciotti (1998). It was found that while SN Ia input sufficed for low- and intermediate-luminosity elliptical galaxies to produce fast galactic winds, the inner parts of more massive spheroids would nevertheless host inflow solutions similar to cooling flows. This is because, while the number of SNe Ia per unit optical luminosity is expected to be roughly constant in ellipticals, the gas binding energy per unit mass increases with galactic luminosity. However, it is not likely that SNe Ia can provide the entire solution to this problem

[1] Department of Astronomy, University of Bologna, I-40127 Bologna, Italy.
[2] Princeton University Observatory, Princeton, NJ 08544.
[3] Institute of Astronomy, University of Cambridge, Cambridge CB3 0HA, UK.

because the distribution of the energy input is not concentrated enough to balance the observed gas cooling rate (since this scales as ρ^2, the required heating rate must be very large in the very central regions). Note also that the SN Ia rate is independent of the current thermal state of the X-ray–emitting plasma; therefore, SN heating cannot act as a self-regulating mechanism. Finally, as already recognized by C91, the mass budget problem would still affect medium-large galaxies, putative hosts of luminous cooling flows. Thus, a concentrated feedback source is a very promising solution for a variety of problems, and the central SMBH is the natural candidate, by its mass and by its location, through a combination of mechanical and radiative feedback mechanisms (see, e.g., Fabian et al. 2006 and references therein).

Some calculations have allowed for a physically motivated AGN feedback (see, e.g., Binney & Tabor 1995; Ciotti & Ostriker 1997, hereafter CO97; Ciotti & Ostriker 2001, hereafter CO01; Omma et al. 2004; Ostriker & Ciotti 2005, hereafter OC05; Churazov et al. 2005), and the computed solutions are characterized by relaxation oscillations (Ostriker et al. 1976; Cowie et al. 1978). Energy output (radiative or mechanical) from the central SMBH pushes matter out, the accretion rate drops precipitously, and the expanding matter drives shocks into the galactic gas. Then the resulting hot bubble ultimately cools radiatively (it is thermally unstable) and the resulting infall leads to renewed accretion; the cycle repeats. Among the computed models that studied the interaction between AGN feedback and galactic cooling flows, those of CO97 and CO01 focused on the effects of *radiative heating* on galactic gas flows. In fact, if one allows the radiation emitted from the accreting SMBH to interact with and heat the galactic gas, one solves the cooling flow problem in elliptical galaxies, and the feedback produces systems that are variable but typically look like normal ellipticals containing hot gas. They sometimes look like incipient cooling flows and rarely, but importantly, appear like quasars. Interestingly, observations seem to support this scenario (e.g., Russell et al. 2007).

In CO97 and CO01, however, a major uncertainty remained about the typical QSO spectrum to adopt, in particular the high-energy component of that spectrum, which is most important for heating the ambient gas. Thus, a simple broken power law was adopted for the spectrum with a range of possible values of the Compton temperature (from $10^{7.2}$ to $10^{9.5}$ K), with most of the emphasis of the paper being on the higher temperatures. Subsequent work by Sazonov et al. (2004; see also Sazonov et al. 2007), which assessed the full range of observational data of AGNs and computed their spectral energy distribution, concluded that the typical equilibrium radiation temperature was narrowly bounded to values near $10^{7.3}$ K, i.e., of the order of 2 keV. This value, although it is at the lower end of the range adopted by CO01, is still above the virial temperature of all galaxies and, most importantly, well above the central temperature of the cooling flow gas. As noted by Sazonov et al. (2005), there is a rather large compensating effect also not included in CO01: gas heated by radiation with a characteristic temperature near 10^7 K is heated far more effectively by absorption in the atomic lines of the abundant metal species than by the Compton process. In particular, Sazonov et al. (2005) provide a fitting formula for the Compton plus photoionization and line heating/cooling that we implemented into our numerical code, together with additional physics that was missing in CO97 and CO01; a very preliminary exploration of the new models can be found in OC05. Consistently with a second generation of metal-rich stars observed in recent SDSS surveys (e.g., Fukugita et al. 2004; Nolan et al. 2007), we now also allow for star formation, which is found to be of primary importance during the first few Gyr, as it consumes a large fraction of the cooling gas in a central starburst (e.g., Reuland et al. 2007).

In this paper we address the coevolution of an SMBH and of the interstellar medium (ISM) of the host galaxy and argue that the AGN/starburst feedback effects can be the answer to the triple problems of (1) the suppression of cooling flows within galaxies, (2) the large scatter in their hot gas mass at fixed optical luminosity, and (3) disposition of the recycled gas. It is found that the intermittences described in CO97 and CO01 are confirmed also with the more accurate treatment of the radiation field, and these have two consequences: they cause nuclear starbursts and they feed the central SMBH in what we observe as coincident AGN/starburst episodes. In addition, since the fuel is in fact proportional to the evolving stellar mass, one maintains, on average, a central SMBH mass and a younger stellar population mass that are both proportional to the galactic stellar mass, with the energetic feedback from central SNe II and AGNs producing the energy input needed to keep the bulk of the gas in a state of low density and high temperature. For simplicity in this paper we just present a summary of the main properties of a typical model, leaving to following papers the detailed description of specific features of observational and theoretical interest.

The paper is organized as follows. In § 2 we describe how the galactic models adopted in the simulations are built, the details of the input physics, and their numerical implementation. In § 3 the time evolution of a representative model galaxy is illustrated in detail. Finally, in § 4 we discuss the main results obtained.

2. THE MODELS

The galactic models and the input physics adopted for the simulations have been substantially improved with respect to CO97 and CO01: in the following we describe them in detail for future reference.

2.1. *Structure and Internal Dynamics*

In CO01 the galactic models utilized a King (1972) stellar distribution plus a quasi-isothermal dark matter halo, in line with the models then used for cooling flow studies. However, the existence of large cores of constant surface brightness has been clearly ruled out (see, e.g., Jaffe et al. 1994; Faber et al. 1997; Lauer et al. 2005), as *Hubble Space Telescope* (*HST*) observations have shown how the central surface brightness profile is described by a power law as far in as it can be observed, i.e., to $\sim$10 pc for Virgo ellipticals. Following Pellegrini & Ciotti (1998), we then adopt a stellar density distribution described by the more appropriate Hernquist (1990) model

$$\rho_* = \frac{M_*}{2\pi}\,\frac{r_*}{r(r+r_*)^3}. \tag{2}$$

Optical (e.g., Saglia et al. 1993; Bertin et al. 1994; Cappellari et al. 2006; Douglas et al. 2007) and X-ray (e.g., Fabian et al. 1986; Humphrey et al. 2006) based studies typically find that luminous matter dominates the mass distribution inside the effective radius R_e, while dark matter begins to be dynamically important at $2R_e$–$3R_e$, with common values of the total dark-to-luminous mass ratio $\mathcal{R} \equiv M_h/M_*$ in the range $1 \lesssim \mathcal{R} \lesssim 6$. Theoretical (e.g., Dubinski & Carlberg 1991; Ciotti & Pellegrini 1992; Navarro et al. 1997; Fukushige & Makino 1997) and observational (e.g., Treu et al. 2006) arguments support the idea that, similarly to the stellar profiles, the radial density distribution of the dark halos is described by a cuspy profile with central spatial

density increasing as r^{-1}: consistently, for the dark matter halo we also adopt the density distribution in equation (2), where $M_h = \mathcal{R}M_*$ and $r_h = \beta r_*$ are the halo total mass and scale length, respectively; dynamical and phase-space properties of the resulting two-component Hernquist models are given in Ciotti (1996).

In order to use realistic galactic models, the mass distribution is determined as follows. We fix a value for the projected central velocity dispersion σ, and we determine the galactic *present-day* model blue luminosity L_B and effective radius R_e from the Faber-Jackson

$$\frac{L_B}{10^{11}\ L_{B\odot}} = 0.23\left(\frac{\sigma}{300\ \mathrm{km\ s^{-1}}}\right)^{2.4} + 0.62\left(\frac{\sigma}{300\ \mathrm{km\ s^{-1}}}\right)^{4.2} \tag{3}$$

and the fundamental plane

$$\log R_e = A\log\sigma + B\log I_e + C \tag{4}$$

relations adopted in C91, where $I_e \equiv L_B/(2\pi R_e^2)$. The scale length r_* of the stellar distribution (eq. [2]) is then given by $r_* \simeq R_e/1.8153$ (Hernquist 1990).

Having fixed σ and r_*, we determine the galaxy stellar mass and halo properties such that σ_a, the model aperture velocity dispersion within $R_e/8$ (obtained by solving and projecting the Jeans equations), coincides with σ. For globally isotropic two-component Hernquist models

$$\sigma_a^2\left(\frac{R_e}{8}\right) \simeq \frac{GM_*}{r_*}\left(0.096 + \frac{0.12\mathcal{R}}{\beta^{1.72}}\right), \tag{5}$$

where

$$\beta \equiv \frac{r_h}{r_*} = \left(1+\sqrt{2}\right)\left(\sqrt{\frac{2\mathcal{R}}{\mathcal{R}_{0.5}}} - 1\right), \tag{6}$$

and $\mathcal{R}_{0.5}$ is the dark-to-visible mass ratio within the stellar half-mass radius (Pellegrini & Ciotti 2006); note that we do not consider the effect of $M_{\rm BH}$ on σ_a, in accordance with estimates of the SMBH sphere of influence radius (e.g., Riciputi et al. 2005). For chosen values of $\mathcal{R}$ and $\mathcal{R}_{0.5}$ we obtain M_* and the stellar mass-to-light ratio $\Upsilon_* \equiv M_*/L_B$ from equations (5) and (6). In the initial conditions we then expand the scale radius r_* thus determined by a factor of 1.5 (while maintaining fixed the dark matter halo distribution and total mass), in order to allow for the subsequent shrinkage of newly formed stars in the galactic central regions (see § 2.3). As discussed in § 4, we do not attempt at this stage to properly follow the dark matter halo contraction, nor the modifications of the velocity dispersion profile consequent to star formation.

An important ingredient in the energetics of the gas flows, namely, the thermalization energy of the stellar mass losses, depends on the radial trend of the stellar velocity dispersion (see § 2.7), which, for the isotropic case, is given (via the Jeans equations) by

$$\rho_*\sigma_*^2 = \rho_*\sigma_*^2(M_{\rm BH}=0) + \frac{GM_*M_{\rm BH}}{2\pi r_*^4} \times\left[6\ln\left(1+\frac{1}{s}\right) - \frac{(1+2s)(6s^2+6s-1)}{2s^2(1+s)^2}\right], \tag{7}$$

where $s \equiv r/r_*$, and the first term on the right-hand side is the one-dimensional stellar velocity dispersion without the contribution of the SMBH (Ciotti et al. 1996).

2.2. *Stellar Passive Evolution: SN Ia Rate and Stellar Mass Losses*

The stellar mass-loss rate and the SN Ia rate associated with the initial stellar distribution are the main ingredients driving evolution of the models. In the code the stellar mass losses—the source of *fuel* for the activity of the SMBH—follow the detailed prescriptions of the stellar evolution theory, while for quick calculations the approximation given in equation (1) can be used. Over the whole galaxy

$$\dot{M}_* = \mathrm{IMF}(M_{\rm TO})\left|\dot{M}_{\rm TO}\right|\Delta M, \tag{8}$$

where the initial mass function (IMF) is a Salpeter law (normalized as described in C91) and the turnoff mass (in $M_\odot$) of stars at time t (in yr) is

$$\log M_{\rm TO} = 0.0558(\log t)^2 - 1.338\log t + 7.764. \tag{9}$$

Finally,

$$\Delta M = \begin{cases} M_{\rm TO} - M_{\rm fin}(M_{\rm TO}) \\ \quad = 0.945M_{\rm TO} - 0.503, & M_{\rm TO} < 9\ M_\odot, \\ \Delta M = M_{\rm TO} - 1.4\ M_\odot, & M_{\rm TO} \geq 9\ M_\odot \end{cases} \tag{10}$$

(C91). Recently, updated formulae have become available (Maraston 2005), but in the present context the modifications on the flow evolution are minor (Pellegrini & Ciotti 2006) and so for continuity we maintained the treatment of past works. Also, SN Ia rates in early-type galaxies have been carefully reanalyzed, and current estimates of the rate in the local universe agree on $0.32h^2$ SNu (where 1 SNu = 1 SN Ia per century per $10^{10}\ L_{B\odot}$ and $h \equiv H_0/100\ \mathrm{km\ s^{-1}\ Mpc^{-1}}$; see, e.g., Cappellaro et al. 1999; Mannucci et al. 2005) so that, following C91, we parameterize the time evolution of the SN Ia rate as

$$R_{\rm SN}(t) = 0.32\times10^{-12}h^2\vartheta_{\rm SN}\frac{L_B}{L_{B\odot}}\left(\frac{t}{13.7\ \mathrm{Gyr}}\right)^{-s}\ \mathrm{yr^{-1}}, \tag{11}$$

where the coefficient $\vartheta_{\rm SN}$ allows for different choices in the present-day SNe Ia. Assuming for each supernova event an energy release of $E_{\rm SN} = 10^{51}$ ergs, a fraction $\eta_{\rm SN}$ of which is thermalized in the surrounding ISM, the energy input per unit time over the entire galaxy body is given by

$$L_{\rm SN}(t) = 1.015\times10^{31}h^2\vartheta_{\rm SN}\eta_{\rm SN}\frac{L_B}{L_{B\odot}}\left(\frac{t}{13.7\ \mathrm{Gyr}}\right)^{-s}\ \mathrm{ergs\ s^{-1}}. \tag{12}$$

In this paper we restrict to the case $\vartheta_{\rm SN} = 1$ and $h = 0.75$. As is well known, the specific value of s is a critical ingredient in the model evolution. In fact, when $s \gtrsim 1.3$, the flow evolves from wind to inflow, while the opposite is true for $s \lesssim 1.3$. This was especially true in C91, CO97, and CO01 models. However, the specific value of s is less important in affecting the evolution of gas flows in cuspier galaxy models with a somewhat reduced SN Ia present-day rate, as those here explored, that preferentially host "partial wind" solutions (Pellegrini & Ciotti 1998). Thus, here we restrict to the currently favored $s = 1.1$ value (Greggio 2005), even though a more complicated time dependence than a simple

power law seems possible (e.g., Matteucci et al. 2006; Neill et al. 2007).

Besides energy, supernovae provide also mass. We assume that each SN Ia ejects 1.4 $M_\odot$ of material in the ISM, so that the total rate of mass return from the aging initial stellar population at each place in the galaxy is

$$\frac{d\rho_*}{dt} = (\alpha_* + \alpha_{\rm SN})\rho_*, \tag{13}$$

where $\alpha_{\rm SN}(t) = 1.4\ M_\odot[R_{\rm SN}(t)/M_*]$ and $\alpha_*(t) = \dot{M}_*(t)/M_*$ are the specific mass return rates. With these definitions, the SN Ia kinetic energy injection per unit volume in the ISM can be written as

$$\dot{E}_{\rm I} = \eta_{\rm SN} E_{\rm SN} \frac{R_{\rm SN}}{M_*}\rho_* = \eta_{\rm SN} E_{\rm SN} \frac{\alpha_{\rm SN}(t)\rho_*}{1.4\ M_\odot}. \tag{14}$$

2.3. *Star Formation, SN II Heating, and Starburst Properties*

At variance with CO01, in the present study we allow for star formation, which cannot be avoided when cool gas accumulates in the central regions of elliptical galaxies. In particular, we compute the star formation rate at each radius r from the equation

$$\dot{\rho}_*^+ = \frac{\eta_{\rm form}\rho}{\tau_{\rm form}}, \quad \tau_{\rm form} = \max\left(\tau_{\rm cool},\ \tau_{\rm dyn}\right), \tag{15}$$

where ρ is the local gas density, $\eta_{\rm form} = 0.03$–0.4 (see, e.g., Weinberg et al. 2002; Cen & Ostriker 2006), and the associated characteristic times are

$$\tau_{\rm cool} \equiv \frac{E}{C}, \quad \tau_{\rm dyn} = \min(\tau_{\rm Jeans},\ \tau_{\rm rot}),$$
$$\tau_{\rm Jeans} \equiv \sqrt{\frac{3}{32\pi G\rho}}, \quad \tau_{\rm rot} \equiv \frac{2\pi r}{v_c(r)}. \tag{16}$$

This formulation is usually termed the "Schmidt-Kennicutt prescription." E and C are the gas internal energy and the effective cooling per unit volume (see eq. [36]), while $v_c(r)$ is the galaxy rotational velocity at radius r. In the code the stars are maintained in the place where they form, and in each shell the associated sinks of momentum and internal energy per unit volume are given by the negative of

$$\dot{\boldsymbol{m}}_*^+ = \frac{\eta_{\rm form}\boldsymbol{m}}{\tau_{\rm form}}, \quad \dot{E}_*^+ = \frac{\eta_{\rm form}E}{\tau_{\rm form}}, \tag{17}$$

where m is the specific momentum of the ISM (see § 2.7).

For a total mass ΔM_* of newly formed stars in a given time step and at a given place we assume a Salpeter IMF

$$\frac{dN}{dM} = (x-1)\left(\frac{M_{\rm inf}}{M_\odot}\right)^{x-1}\frac{\Delta M_*}{M_\odot}\left(\frac{M}{M_\odot}\right)^{-1-x} \tag{18}$$

($x > 1$, $M \geq M_{\rm inf} = 0.1\ M_\odot$), so that the associated total number of SNe II is

$$N_{\rm II} = \int_{M_{\rm II}=8\ M_\odot}^{\infty}\frac{dN}{dM}\,dM = \left(1-\frac{1}{x}\right)\left(\frac{M_{\rm inf}}{M_{\rm II}}\right)^x\frac{M_\odot}{M_{\rm inf}}\frac{\Delta M_*}{M_\odot}$$
$$\simeq 7\times10^{-3}\frac{\Delta M_*}{M_\odot}, \tag{19}$$

where the numerical value holds for $x = 1.35$. As for SNe Ia, we assume that each SN II event releases $E_{\rm SN} = 10^{51}$ ergs of kinetic energy, and the resulting mean efficiency is

$$\epsilon_{\rm II} \equiv \frac{N_{\rm II}E_{\rm SN}\eta_{\rm SN}}{\Delta M_* c^2}$$
$$= \left(1-\frac{1}{x}\right)\left(\frac{M_{\rm inf}}{M_{\rm II}}\right)^x\frac{M_\odot}{M_{\rm inf}}\frac{E_{\rm SN}\eta_{\rm SN}}{M_\odot c^2} \simeq 3.9\times10^{-6}\eta_{\rm SN}. \tag{20}$$

In this paper we assume $\eta_{\rm SN} = 0.85$. The characteristic time for SN II explosion is fixed to $\tau_{\rm II} = 2\times10^7$ yr, and from equations (15) and (20) their luminosity (per unit volume) at each radius from the galactic center is

$$\dot{E}_{\rm II}(t) \equiv \frac{\epsilon_{\rm II}c^2}{\tau_{\rm II}}\int_0^t \dot{\rho}_*^+(t')e^{-(t-t')/\tau_{\rm II}}\,dt'. \tag{21}$$

We assume that each explosion leaves neutron stars of 1.4 $M_\odot$; another possibility would be to assume more massive BH remnants (see, e.g., Renzini & Ciotti 1993). As a consequence, the total mass ejected by the SN II explosions per unit mass is

$$\frac{M_{\rm II}^{\rm ej}}{\Delta M_*} = \left(\frac{M_{\rm inf}}{M_{\rm II}}\right)^{x-1} - 1.4\frac{N_{\rm II}M_\odot}{\Delta M_*} \simeq 0.2, \tag{22}$$

and the mass return rate per unit volume of the young evolving stellar population is given by

$$\dot{\rho}_{\rm II}(t) \simeq \frac{0.2}{\tau_{\rm II}}\int_0^t \dot{\rho}_*^+(t')e^{-(t-t')/\tau_{\rm II}}\,dt'. \tag{23}$$

Finally, in the code we also compute the fiducial optical and UV luminosity per unit volume of the new stars as

$$\dot{E}_{\rm opt}(t) \equiv \frac{\epsilon_{\rm opt}c^2}{\tau_{\rm opt}}\int_0^t \dot{\rho}_*^+(t')e^{-(t-t')/\tau_{\rm opt}}\,dt' \tag{24}$$

and

$$\dot{E}_{\rm UV}(t) \equiv \frac{\epsilon_{\rm UV}c^2}{\tau_{\rm UV}}\int_0^t \dot{\rho}_*^+(t')e^{-(t-t')/\tau_{\rm UV}}\,dt', \tag{25}$$

respectively, where $\epsilon_{\rm opt} = 1.24\times10^{-3}$, $\epsilon_{\rm UV} = 8.65\times10^{-5}$, $\tau_{\rm opt} = 1.54\times10^8$ yr, and $\tau_{\rm UV} = 2.57\times10^6$ yr are the efficiency and characteristic time of optical and UV emission, respectively. The time delay equations (21) and (23)–(25) are integrated according to the scheme described in the Appendix.

2.4. *The Circumnuclear Disk and the SMBH Accretion Luminosity*

At the onset of the cooling catastrophe a large amount of gas suddenly flows onto the central regions of the galaxy, and this induces star formation and accretion on the central SMBH, producing a burst of energy from the galactic center. However, observations of our own Galactic center and high-resolution studies of other nearby systems indicate that, in addition to the central starburst with radius ~100–300 pc, accretion onto the central SMBH is mediated by a small central disk within which additional significant star formation occurs (see, e.g., Goodman & Tan 2004; Tan & Blackman 2005; see also Kawata et al. 2007), and the remaining fraction of gas either is blown out in a broad-line wind or is accreted onto the central SMBH. In our code the disk is not simulated with hydrodynamical equations, but its modelization is needed to obtain important quantities required

by the code. The disk, which is the repository of the gas inflowing at a rate $\dot{M}_1$ from the first active grid point R_1 of the hydrodynamical grid[4] and which feeds the central SMBH at a rate $\dot{M}_{\rm BH}$, contains at any time the gas mass m_g and a total stellar mass $m_* = m_{*l} + m_{*h}$, which is divided among low- and high-mass stars. Finally, the disk also contains a mass $m_{\rm rem}$ of remnants from the earlier generations of evolved stars.

In the adopted scheme the accretion rate on the central SMBH is given by

$$\dot{M}_{\rm BH} = \frac{\dot{m}_{\rm fid}}{1+\eta_d}, \quad \eta_d \equiv \frac{\dot{m}_{\rm fid}}{2\dot{m}_{\rm Edd}}, \tag{26}$$

where

$$\dot{m}_{\rm fid} \equiv \frac{m_g}{\tau_{\rm lag}}, \quad \dot{m}_{\rm Edd} \equiv \frac{L_{\rm Edd}}{\epsilon c^2}, \tag{27}$$

are the fiducial depletion rate of gas from the circumnuclear disk and the Eddington mass accretion rate, respectively, while the characteristic disk star formation time $\tau_{\rm lag}$ is defined as

$$\tau_{\rm lag} \equiv \frac{2\pi}{\alpha}\sqrt{\frac{R_1^3}{GM_{\rm BH}}}, \tag{28}$$

where $\alpha \simeq 10^{-2}$ to 10^{-1} (or higher; see, e.g., King et al. 2007) is the disk viscosity coefficient. More rigorous formulations of $\tau_{\rm lag}$ are possible, but at the current level of modelization equation (28) is accurate enough. Thus, equations (26) and (27) guarantee that when $\eta_d \ll 1$, the gas is accreted onto the central SMBH at the rate $\dot{m}_{\rm fid}$, while $\dot{M}_{\rm BH} = 2\dot{m}_{\rm Edd}$ for $\eta_d \gg 1$ (the factor of $\frac{1}{2}$ in the definition of η_d allowing for possible super-Eddington accretion); note, however, that outside the first grid point R_1 the flow accretion rate is limited in a self-consistent way by radiation pressure (see §§ 2.6 and 2.7).

We also assume that a fraction of the disk gas mass is converted into stars at a rate $\eta_*\dot{m}_{\rm fid}$ (where $\eta_* \simeq 10 m_g/M_{\rm BH}$, to approximate a Toomre criterion for star formation in the disk) and that another fraction of m_g is lost as a wind at an instantaneous rate given by $\eta_w \dot{M}_{\rm BH}$ (with $\eta_w = 2$, so that the broad-line wind carries away twice as much mass as falls to the SMBH), so that the equation for the gas mass in the disk is

$$\frac{dm_g}{dt} = \dot{M}_1 - (1+\eta_w)\dot{M}_{\rm BH} - \eta_*\dot{m}_{\rm fid}. \tag{29}$$

The stars formed in the disk are described separately as a function of their mass; i.e., high-mass stars ($M > M_{\rm II} = 8\ M_\odot$) produce a total disk mass m_{*h}, and low-mass stars ($M_{\rm inf} < M < M_{\rm II}$) contribute to a disk mass m_{*l} according to the equations

$$\frac{dm_{*l}}{dt} = (1-f_h)\eta_*\dot{m}_{\rm fid} - \frac{m_{*l}}{\tau_{*l}}, \quad \frac{dm_{*h}}{dt} = f_h\eta_*\dot{m}_{\rm fid} - \frac{m_{*h}}{\tau_{*h}}, \tag{30}$$

where for the characteristic evolutionary times we adopt $\tau_{*l} = \tau_{\rm opt}$ and $\tau_{*h} = \tau_{\rm II}$ given in § 2.3, while we assume $f_h = 0.5$, corresponding to a top-heavy Salpeter-like IMF of slope $x \simeq 1.16$ and minimum mass $M_{\rm inf} = 0.1\ M_\odot$ (see eq. [18]).[5] The associated optical ($L_{d,\rm opt}$) and UV ($L_{d,\rm UV}$) luminosities of the stellar disk are calculated following the scheme of § 2.3. Finally, stellar remnant mass in the disk evolves as

$$\frac{dm_{\rm rem}}{dt} = f_{{\rm rem},l}\frac{m_{*l}}{\tau_{*l}} + f_{{\rm rem},h}\frac{m_{*h}}{\tau_{*h}}, \tag{31}$$

where $f_{{\rm rem},l} = 0.2$, $f_{{\rm rem},h} = 0.09$. Thus, the equation for the mass of the disk wind is

$$\frac{dm_w}{dt} = \eta_w\dot{M}_{\rm BH} + \left(1-f_{{\rm rem},l}\right)\frac{m_{*l}}{\tau_{*l}} + \left(1-f_{{\rm rem},h}\right)\frac{m_{*h}}{\tau_{*h}}. \tag{32}$$

The first term is a mass loss driven by the central SMBH, and the second and third are from high- and low-mass stars in the central disk. All the equations in this section are integrated with a first-order finite-difference scheme.

From equation (26) we calculate the electromagnetic bolometric accretion luminosity as

$$L_{\rm BH}(t) = \epsilon\dot{M}_{\rm BH}(t)c^2, \tag{33}$$

where the radiative efficiency ϵ usually spans the range $0.001 \lesssim \epsilon \lesssim 0.15$. We adopt $\epsilon = 0.1$ in the present paper, consistent with observations (see, e.g., Soltan 1982; Yu & Tremaine 2002; Haiman et al. 2004), but a generalization to include an ADAF-like efficiency could also be easily implemented in the code (Narayan & Yi 1994; see also CO01).

We also compute a fiducial mechanical luminosity for the disk wind $L_{\rm dw}$, defined as

$$L_{\rm dw} = \epsilon_{{\rm BH},w}\dot{M}_{\rm BH}c^2 + \epsilon_{\rm II}c^2\left(1-f_{{\rm rem},h}\right)\frac{m_{*h}}{\tau_{*h}}, \tag{34}$$

where $\epsilon_{{\rm BH},w} = 5\times10^{-4} = 0.005\epsilon$ is the mechanical efficiency of the SMBH (Elvis 2006). This mechanical energy output is a factor of 10 lower than adopted by Hernquist and collaborators when described in the same units, and adding this mechanical output to our simulation would be only a slight correction, since $\epsilon_{{\rm BH},w}/\epsilon \sim 0.5\%$. The associated disk wind velocity is then given by

$$v_w \equiv \sqrt{\frac{2L_{\rm dw}}{\dot{m}_w}} \simeq \sqrt{\frac{2\epsilon_{{\rm BH},w}}{\eta_w}}c \simeq 7\times10^3\ {\rm km\ s^{-1}} \tag{35}$$

for our parameters, in agreement with observations of broad-line regions.

In summary, the mass falling to the center is mediated by a gaseous, star-forming α-disk that surrounds the SMBH. A small fraction of the mass is turned into (primarily) high-mass stars in the disk, roughly two-thirds is expelled in the broad-line wind, and roughly one-third is accreted onto the central SMBH.

2.5. *Radiative Heating and Cooling*

With an improvement over CO01, the radiative heating and cooling produced by the accretion luminosity are numerically computed by using the Sazonov et al. (2005) formulae, which describe the net heating/cooling rate per unit volume $\dot{E}$ of a cosmic plasma in photoionization equilibrium with a radiation field characterized by the average quasar spectral energy distribution by Sazonov et al. (2004), whose associated spectral temperature is $T_{\rm X} \simeq 2$ keV. In particular, Compton heating and cooling, bremsstrahlung losses, and line and recombination continuum heating and cooling are taken into account.

[4] $\dot{M}_1$ is taken to be positive in the case of accretion and zero in the case of outflow at R_1.

[5] The choice of a top-heavy IMF for the disk stars, at variance with the standard Salpeter law adopted for the new stars formed over the galaxy body, is motivated, for example, by the dynamical and X-ray evidences reported in Nayakshin & Sunyaev (2005) and Nayakshin et al. (2006).

A good approximation to the net gas energy change rate $\dot{E}$, valid for $T \gtrsim 10^4$ K (all quantities are expressed in the cgs system), is given by

$$\dot{E} = n^2(S_1 + S_2 + S_3) \equiv H - C, \tag{36}$$

where n is the hydrogen density (in number), and positive and negative terms are grouped together in the heating (H) and cooling (C) functions. The bremsstrahlung losses are given by

$$S_1 = -3.8 \times 10^{-27}\sqrt{T}, \tag{37}$$

the Compton heating and cooling are given by

$$S_2 = 4.1 \times 10^{-35}(T_X - T)\xi, \tag{38}$$

where T_X is the Compton temperature, and finally the sum of photoionization heating and line and recombination continuum cooling is

$$S_3 = 10^{-23}\frac{a + b(\xi/\xi_0)^c}{1 + (\xi/\xi_0)^c}, \tag{39}$$

where

$$a = -\frac{18}{e^{25(\log T - 4.35)^2}} - \frac{80}{e^{5.5(\log T - 5.2)^2}} - \frac{17}{e^{3.6(\log T - 6.5)^2}}, \tag{40}$$

$$b = 1.7 \times 10^4 T^{-0.7}, \tag{41}$$

$$c = 1.1 - \frac{1.1}{e^{T/1.8\times 10^5}} + \frac{4\times 10^{15}}{T^4}, \tag{42}$$

and

$$\xi_0 = \frac{1}{1.5T^{-0.5} + 1.5\times 10^{12}T^{-2.5}} + \frac{4\times 10^{10}}{T^2}\left(1 + \frac{80}{e^{(T-10^4)/1.5\times 10^3}}\right). \tag{43}$$

Equations (38) and (39) depend on the ionization parameter

$$\xi \equiv \frac{L^{\rm eff}_{\rm BH,\,photo}(r)}{n(r)r^2}, \tag{44}$$

where $L^{\rm eff}_{\rm BH,\,photo}(r)$ is the effective accretion luminosity at r, which is evaluated by numerically solving in each shell the balance equation

$$\frac{dL^{\rm eff}_{\rm BH,\,photo}(r)}{dr} = -4\pi r^2 H, \tag{45}$$

with central boundary condition $L^{\rm eff}_{\rm BH,\,photo}(r=0) = L_{\rm BH}(t)$ given by equation (33). The photoionization+Compton opacity associated with radiation absorption is then obtained:

$$\kappa_{\rm photo} = -\frac{1}{\rho L^{\rm eff}_{\rm BH,\,photo}(r)}\frac{dL^{\rm eff}_{\rm BH,\,photo}(r)}{dr} = \frac{4\pi r^2 H(r)}{\rho(r) L^{\rm eff}_{\rm BH,\,photo}(r)}. \tag{46}$$

Finally, the bolometric ISM luminosity is obtained from equation (36) as

$$L_r(r) = 4\pi\int_0^r Cr^2\,dr. \tag{47}$$

The essential physics of this section is well known. When the parameter ξ is large, thermodynamics guarantees that the gas temperature approaches the photoionization temperature $\sim 10^{7.3}$ K, but for lower values of ξ the temperature approaches $\sim 10^4$ K, near the peak of the cooling curve.

2.6. *Radiation Pressure*

An important ingredient in the modelization of the gas flow evolution is the radiation pressure due to the accretion luminosity and to the light produced by the new stars. In its evaluation the explicit dependence on time is omitted, since the light-travel time in the regions of interest is small compared to the timescale on which the radiative input changes. Radiation pressure due to *electron scattering* (where neither the photon numbers nor their energy change) is computed as

$$(\nabla p_{\rm rad})_{\rm es} = -\frac{\kappa_{\rm es}\rho}{c}\frac{L_{\rm BH} + L_{\rm UV}(r) + L_{\rm opt}(r) + L_{\rm r}(r)}{4\pi r^2}, \tag{48}$$

where $\kappa_{\rm es} = 0.35$ in cgs units, and from equations (24) and (25)

$$L_{\rm UV}(r) = 4\pi\int_0^r \dot{E}_{\rm UV} r^2\,dr, \quad L_{\rm opt}(r) = 4\pi\int_0^r \dot{E}_{\rm opt} r^2\,dr. \tag{49}$$

Note that all the luminosities used in equation (48) are unabsorbed.

The radiation pressure contribution due to *dust opacity* is given by

$$(\nabla p_{\rm rad})_{\rm dust} = -\frac{\kappa_{\rm UV}\rho}{c}\frac{L^{\rm eff}_{\rm BH,UV}(r) + L^{\rm eff}_{\rm UV}(r)}{4\pi r^2} - \frac{\kappa_{\rm opt}\rho}{c}\frac{L^{\rm eff}_{\rm BH,opt}(r) + L^{\rm eff}_{\rm opt}(r)}{4\pi r^2} - \frac{\kappa_{\rm IR}\rho}{c}\frac{L_{\rm IR}(r)}{4\pi r^2}, \tag{50}$$

where

$$L_{\rm IR}(r) \equiv L^{\rm abs}_{\rm BH,UV}(r) + L^{\rm abs}_{\rm BH,opt}(r) + L^{\rm abs}_{\rm UV}(r) + L^{\rm abs}_{\rm opt}(r) \tag{51}$$

is the infrared luminosity due to recycling of photons absorbed from the ISM, and we adopt as estimates for (cgs) opacity in three bands

$$\kappa_{\rm opt} = \frac{300}{1 + T/10^4}, \quad \kappa_{\rm UV} = 4\kappa_{\rm opt}, \quad \kappa_{\rm IR} = \frac{\kappa_{\rm opt}}{150}, \tag{52}$$

where the temperature-dependent denominator is designed to mimic the destruction of dust at high temperatures (T. Thompson & B. Draine 2006, private communication); the dust opacity we are using is likely a lower bound to the true value, while a more accurate treatment can be found in Thompson et al. (2005) and will be implemented in future explorations. At variance with electron scattering, the *effective* luminosities appearing in equations (50) and (51) take into account absorption and are obtained by numerically solving the two lowest spherically symmetric

moment equations of radiative transfer in the Eddington approximation (e.g., Chandrasekhar 1960):

$$\frac{dL_{\rm UV}^{\rm eff}}{dr} = 4\pi r^2\left(\dot{E}_{\rm UV} - \kappa_{\rm UV}\rho J_{\rm UV}^{\rm eff}\right),$$
$$\frac{dL_{\rm opt}^{\rm eff}}{dr} = 4\pi r^2\left(\dot{E}_{\rm opt} - \kappa_{\rm opt}\rho J_{\rm opt}^{\rm eff}\right), \quad (53)$$

$$\frac{dJ_{\rm UV}^{\rm eff}}{dr} = -\frac{3\kappa_{\rm UV}\rho L_{\rm UV}^{\rm eff}}{4\pi r^2}, \quad \frac{dJ_{\rm opt}^{\rm eff}}{dr} = -\frac{3\kappa_{\rm opt}\rho L_{\rm opt}^{\rm eff}}{4\pi r^2}. \quad (54)$$

The central boundary conditions for stellar luminosities are $L_{\rm UV}^{\rm eff}(0) = L_{d,\rm UV}$, $L_{\rm opt}^{\rm eff}(0) = L_{d,\rm opt}$, $J_{\rm UV}^{\rm eff}(0) = L_{d,\rm UV}/16\pi^2 R_{\rm I}^2$, and $J_{\rm opt}^{\rm eff}(0) = L_{d,\rm opt}/16\pi^2 R_{\rm I}^2$ (see § 2.4).

The effective accretion luminosities $L_{\rm BH,UV}^{\rm eff}$ and $L_{\rm BH,opt}^{\rm eff}$ are computed with two equations similar to equation (53), where the distributed source term is missing, $J = L_{\rm BH}^{\rm eff}/4\pi r^2$, and in the UV and optical bands $L_{\rm BH,UV}^{\rm eff}(0) = 0.2L_{\rm BH}(t)$ and $L_{\rm BH,opt}^{\rm eff}(0) = 0.1L_{\rm BH}(t)$, respectively.

The last contribution to radiation pressure comes from *photoionization opacity*,

$$(\nabla p_{\rm rad})_{\rm photo} = -\frac{\rho\kappa_{\rm photo}}{c}\frac{L_{\rm BH,\,photo}^{\rm eff}(r)}{4\pi r^2}, \quad (55)$$

where the photoionization opacity and the absorbed accretion luminosity are calculated as described in § 2.5. It is well known that the radiation pressure on electrons (eq. [48]) can significantly affect the gas dynamics when the AGN luminosity approaches the Eddington limit. Consistently with the findings of Thompson et al. (2007), we also find that the radiation pressure on the dust can have a major effect during starburst phases in retarding the infall of cool gas, thus boosting the mass transformed into stars and reducing the gas available for accretion onto the central SMBH.

2.7. *Hydrodynamical Equations*

As in CO01, the evolution of the galactic gas flows is obtained integrating the time-dependent Eulerian equations of hydrodynamics, where now we have several additional source and sink terms

$$\frac{\partial\rho}{\partial t} + \nabla\cdot(\rho\boldsymbol{v}) = \alpha\rho_* + \dot{\rho}_{\rm II} - \dot{\rho}_*^+, \quad (56)$$

$$\frac{\partial m}{\partial t} + \nabla\cdot(\boldsymbol{m}\boldsymbol{v}) = -(\gamma-1)\nabla E - \nabla p_{\rm rad} + \boldsymbol{g}\rho - \dot{\boldsymbol{m}}_*^+, \quad (57)$$

$$\frac{\partial E}{\partial t} + \nabla\cdot(E\boldsymbol{v}) = -(\gamma-1)E\nabla\cdot\boldsymbol{v} + H - C + \frac{(\alpha\rho_* + \dot{\rho}_{\rm II})(v^2 + 3\sigma_*^2)}{2} + \dot{E}_{\rm I} + \dot{E}_{\rm II} - \dot{E}_*^+. \quad (58)$$

Here ρ, $\boldsymbol{m}$, and E are the gas mass, momentum, and internal energy per unit volume, respectively, and v is the gas velocity. The ratio of the specific heats is $\gamma = 5/3$, and $g(r)$ is the gravitational field of the galaxy (stars and dark matter), plus the contribution of the central SMBH. The gravitational field is updated at each time step by considering the SMBH mass growth; for simplicity, we do not take into account either the ISM contribution or the mass redistribution due to the stellar mass losses and star formation. The total radiative pressure gradient is $\nabla p_{\rm rad} = (\nabla p_{\rm rad})_{\rm es} + (\nabla p_{\rm rad})_{\rm dust} + (\nabla p_{\rm rad})_{\rm photo}$ (§ 2.6), while the radiative heating and cooling term $H - C$ is described in § 2.5.

The energy source term is obtained under the assumption that the streaming velocity of the source distribution is zero, neglecting the small contributions of the internal energy of the injected gas and of the kinetic energy of stellar wind when compared to the local stellar velocity dispersion contribution (for the derivation and detailed discussion of the hydrodynamical equations with moving isotropic or anisotropic source terms, see D'Ercole et al. 2000). Note that the term proportional to the stellar velocity dispersion becomes dominant near the SMBH, as described in equation (7). The source terms $\alpha\rho_*$ and $\dot{E}_{\rm I}$ of the initial, passively evolving stellar population are given in equations (13) and (14), while the source terms due to SNe II, $\dot{\rho}_{\rm II}$ and $\dot{E}_{\rm II}$, are described in § 2.3.

From the numerical point of view, the code is the same as in CO97 and CO01; however, the present simulations are much more difficult to run because the stellar density distribution, being more concentrated than the King model, now injects more gas into the central regions, thus increasing the gas density and decreasing its cooling time. In addition, the gas at the galactic center is gravitationally more bound (due to higher mass concentration of the new models) and correspondingly more difficult to expel. Finally, the numerical grid spacing has been reduced in order to resolve the central regions of the galaxy. In particular, we place the first active grid point R_1 within the Compton radius

$$R_{\rm X} = \frac{2GM_{\rm BH}\mu m_p}{3k_{\rm B}T_{\rm X}} \simeq 3.6\mu\frac{M_{\rm BH}}{10^8\ M_\odot}\frac{10^7\ {\rm K}}{T_{\rm X}}\ {\rm pc}, \quad (59)$$

so that at R_1 we can impose the physical condition of a vanishing *thermodynamical* pressure gradient, leading to gas free fall on the circumnuclear disk when the radiation pressure is negligible; in this paper we adopt $T_{\rm X} = 2.5\times10^7$ K. The appropriate values for radiation pressure at R_1 are obtained from the disk treatment described in §§ 2.4 and 2.6. Note that in CO01 we were not able to perform a full simulation with such high resolution, as a consequence of the higher $T_{\rm X}$ adopted.

The simulations are realized with a spatially second-order Eulerian scheme that adopts two staggered grids (for scalar and vector quantities; see C91 and CO01 for details), each of them consisting of 120 logarithmically spaced grid points, covering the range 2.5 pc–200 kpc. The equations are integrated with a time-splitting scheme, while the heating and cooling terms in the energy equation are integrated by using a predictor-corrector scheme, so that the integration is second order in time. At each simulation time, the time step is determined as a fraction of the minimum among the Courant condition over the grid, and of the others characteristic times associated with the described physical processes: during the accretion phases (and subsequent bursts of radiation), it is not infrequent to have time steps of the order of 1 yr or less. However, it is important to note that the accretion events are characterized by the intrinsic timescale related to equation (59) by

$$t_{\rm X} \equiv \frac{R_{\rm X}}{c_{\rm X}} \simeq 1.22\times10^4\mu^{3/2}\frac{M_{\rm BH}}{10^8\ M_\odot}\left(\frac{10^7\ {\rm K}}{T_{\rm X}}\right)^{3/2}\ {\rm yr}, \quad (60)$$

where $c_{\rm X}$ is the isothermal sound velocity associated with the Compton temperature.

3. MODEL EVOLUTION

We now show the main properties of a representative model characterized by an initial stellar mass $M_* = 4.6\times10^{11}\ M_\odot$, FP effective radius $R_e = 6.9$ kpc, aperture velocity dispersion $\sigma_a = 260$ km s^{-1} (leading to an expanded initial condition of $R_e = 10.35$ kpc and $\sigma_a = 235$ km s^{-1}), total dark-to-visible mass ratio $\mathcal{R} = 5$, and dark-to-visible scale length ratio $\beta = 5.22$ (corresponding to an identical amount of stellar and dark matter within

the half-light radius). The initial SMBH mass follows the present-day Magorrian relation, i.e., $M_{\rm BH} \simeq 10^{-3} M_*$. We remark again that this model galaxy is not fully appropriate as an initial condition for a cosmological simulation because its parameters are fixed to reproduce an early-type galaxy similar to those observed in the local universe, and also because we set outflow boundary conditions at the galaxy outskirsts ($\sim$200 kpc): from this point of view, the simulations represent an isolated elliptical galaxy (note, for example, that in the present context we are not considering the effects of possible merging on the galaxy evolution). We adopted this procedure to adhere to the standard approach followed in "cooling flow" simulations, while in future explorations we will address in a more consistent way the problem of the galaxy structural and dynamical modifications due to star formation and mass redistribution over a Hubble time, as well as the compatibility of the obtained galaxies with the present-day scaling laws of elliptical galaxies. We remark that the model presented is just one out of several tens of runs that have been made, characterized by different choices of the parameters (often outside the currently accepted ranges), for example, with high/null DM, enhanced/suppressed star formation, vanishing efficiencies, and so on. The obtained model evolution can be very different, some of them leading to galaxies in a permanent wind state, or galaxies with extremely massive final SMBHs. A discussion of these issues is deferred to successive works.

The initial conditions are represented by a very low density gas at the local virial temperature. The establishment of such high-temperature gas phase at early cosmological times is believed to be due to a "phase transition" when, as a consequence of star formation, the gas-to-stellar mass ratio was of the order of 10% and the combined effect of SN Ia explosions and AGN feedback became effective in heating the gas and driving galactic winds (see, e.g., Sazonov et al. 2005; Tremonti et al. 2007). Several theoretical arguments and much empirical evidence, such as galactic evolutionary models and the metal content of the intracluster medium (ICM), support this scenario (e.g., Renzini et al. 1993; OC05; Di Matteo et al. 2005). For the reasons above, in the simulation presented here (as well as in all other simulations not shown), we assume that the age of the galactic stellar component at the beginning of the simulation is 2 Gyr old, and the simulations span 12 Gyr, so that the cosmic time at the end of the simulations is 14 Gyr.

3.1. *Luminosities*

A first, important result of the new models is that overall the main properties of the CO01 models are confirmed. After a first evolutionary phase in which a galactic wind is sustained by the combined heating of SNe Ia and thermalization of stellar velocity dispersion, the central "cooling catastrophe" commences. In absence of the central SMBH a "mini-inflow" would be then established, with the flow stagnation radius (i.e., the radius at which the flow velocity is zero) of the order of a few hundred parsecs to a few kiloparsecs. These "decoupled" flows are a specific feature of cuspy galaxy models with moderate SN Ia heating (Pellegrini & Ciotti 1998). However, after the central cooling catastrophe, the feedback caused by photoionization and Compton heating strongly affects the subsequent evolution, as can be seen in Figure 1, where we show the luminosity evolution of the central AGN with time sampling of 10^5 yr. The bolometric luminosity (*top panel*) ranges between roughly 0.1 and 0.001 of the Eddington limit (*almost horizontal solid line*) at peaks in the SMBH output, but since obscuration is often significant, the optical accretion luminosity as seen from infinity can be much lower still (*bottom panel*). But the central quasar is not always obscured and

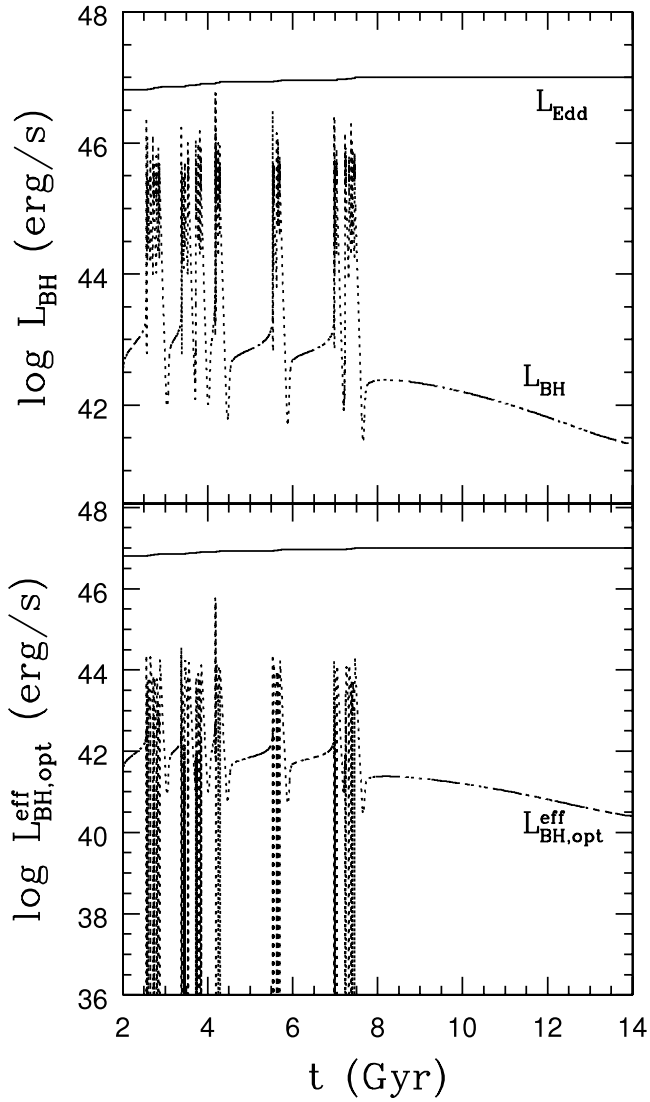

FIG. 1.—Dotted lines are the bolometric accretion luminosity (*top*) and the optical SMBH luminosity corrected for absorption $L^{\rm eff}_{\rm BH,\,opt}$, i.e., as would be observed from infinity (*bottom*; see § 2.6); we recall that at the center we fixed $L^{\rm eff}_{\rm BH,\,opt}(R_1) = 0.1 L_{\rm BH}$. The almost horizontal solid line is $L_{\rm Edd}$.

we see, in the bottom panel of Figure 1, that the optical luminosity reaches $\sim 10^{44}$ ergs s^{-1} in numerous bursts. As already found in CO01, the major AGN outbursts are separated by increasing intervals of time (set by the cooling time) and present a characteristic temporal substructure, whose origin is due to the cooperating effect of direct and reflected shock waves. At $t \simeq 8$ Gyr the SN Ia heating, also sustained by a last strong AGN burst, becomes dominant, a global galactic wind takes place, and the nuclear accretion switches to the optically thin regime. Note that a further reduction of the accretion luminosity during this phase would be obtained if considering ADAF accretion instead of standard accretion.

The temporal substructure of the first major burst is revealed in Figure 2*a*, where we show a blowup of 500 Myr of the top panel of Figure 1, starting at 2.5 Gyr: the time extent of each of the subbursts (for example, when $L_{\rm BH} > 10^{45}$ ergs s^{-1}) is of the order of $\lesssim$1 Myr. In Figures 2*b* and 2*c* we also show the time evolution of the different model opacities during the same burst, where the transition from the optically thin to the optically thick and back to thin phase is apparent.

In Figure 3*a* we show the coronal X-ray luminosity $L_{\rm X}$ (emitted by gas at $T \geq 5 \times 10^6$ K), due to the hot galactic atmosphere

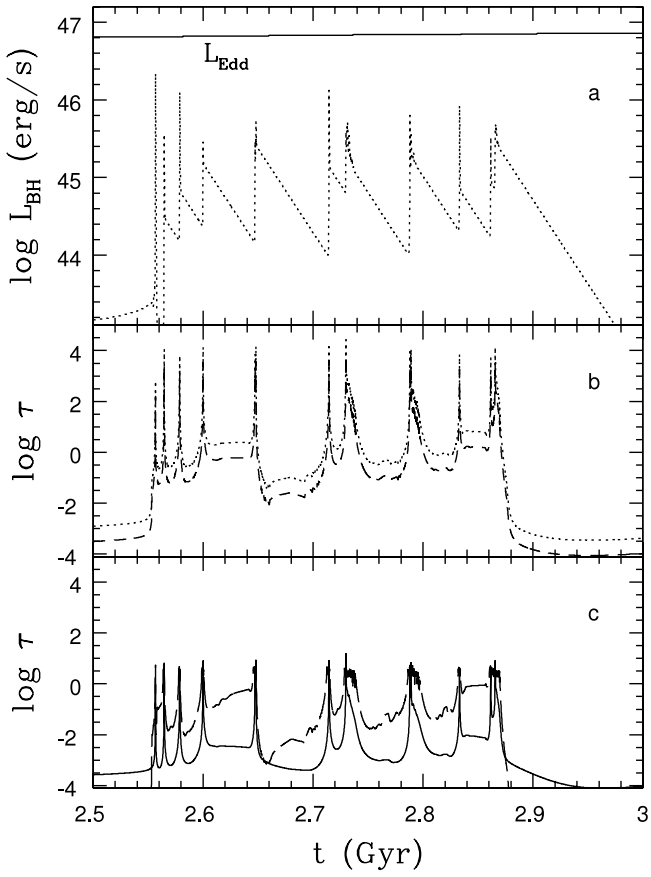

FIG. 2.—(*a*) Time expansion of 500 Myr of the top panel of Fig. 1, showing the first major burst. The dotted line is the *bolometric* accretion luminosity. The widths of the spikes are typically of the order of ∼0.1–1 Myr. (*b*, *c*) Total opacities (defined as $\tau = \int_0^{R_t} \kappa\rho\, dr$, where $R_t = 200$ kpc) of dust on UV (*dotted line*) and optical (*dashed line*) luminosities and on electron scattering (*solid line*) and photoionization opacity (*long-dashed line*), respectively. Dust opacity on the IR recycled radiation would be a line parallel to those in (*b*), but ∼2 orders of magnitude lower (see eq. [52]). Note that the vertical scale is the same in panels (*b*) and (*c*).

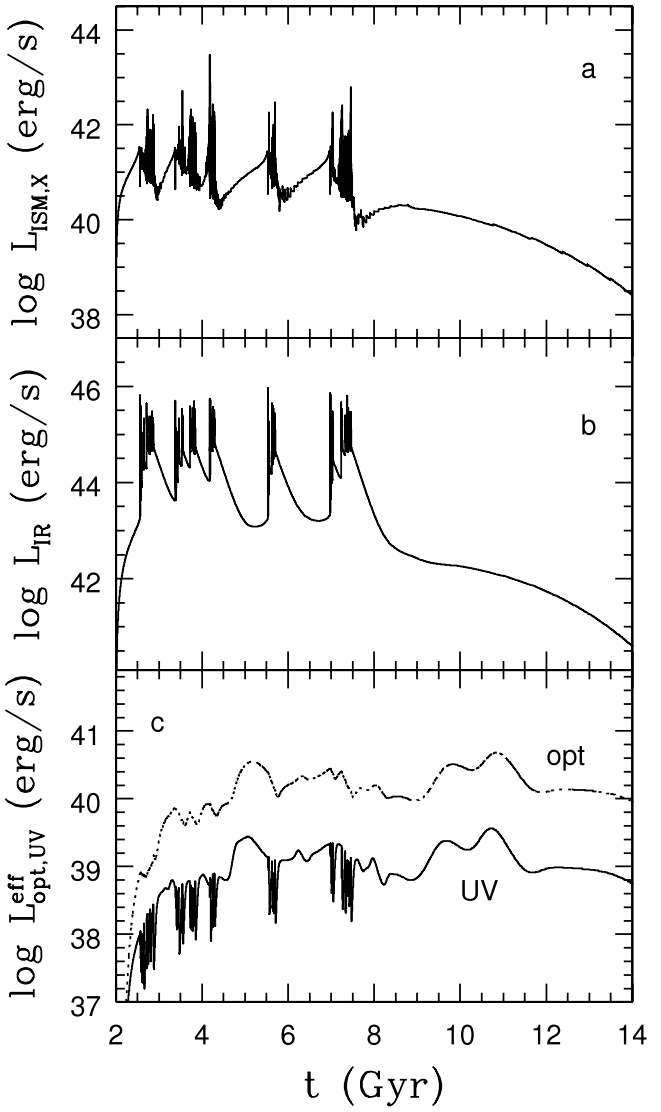

FIG. 3.—Galactic X-ray coronal luminosity L_X (*top*), recycled infrared luminosity L_{IR} (*middle*), and the starburst UV and optical luminosities (*bottom*), corrected for absorption.

integrated within $10R_e$. In particular, L_X falls in the range commonly observed in massive early-type galaxies, with mean values lower than the expected luminosity for a standard cooling flow model. In Figure 3*b* we show instead the estimated IR luminosity L_{IR} due to the reprocessing of the radiation emitted by the new stars and by the SMBH and absorbed by the ISM inside $10R_e$ (eq. [51]). The simulations show that the bulk of the reprocessed radiation comes from AGN obscuration, while the lower envelope is set by radiative reprocessing from the new stars. The very high luminosity peaks ($L_{IR} \sim 10^{45}$–10^{46} ergs s^{-1}) correspond to one component of the SCUBA sources seen at $z \sim 2$ (see, e.g., Pope et al. 2006). Finally, in Figure 3*c* we show the temporal evolution of the optical and UV luminosities of the starbursts corrected for absorption. Overall, Figures 3*b* and 3*c* show that a large fraction of the starburst luminosity output occurs during phases when shrouding by dust is significant (see, e.g., Rodighiero et al. 2007), i.e., the model would be observed as an IR source with UV and optical in the range seen in brighter E+A sources.

The spatial radius within which half of the IR and X-ray luminosities are emitted changes dramatically with time, and as a function of the total emitted luminosity. This is apparent from Figure 4, where we show the time evolution of $r_{h,X}$ and $r_{h,IR}$. Note the large variation of the size of the emission regions: in particular, the smallest values of the half-light radii correspond to the peaks of the associated luminosities. During strong radiation outbursts, the emitting regions are so small (∼10 pc or less) that virtually the entire X-ray and IR luminosities would be seen as emitted by the central source; these phases also correspond to phases of high obscuration, with optical depth of the order of 100 (e.g., Imanishi et al. 2007). Instead, during the late-time hot accretion phase $r_{h,X}$ reaches values commonly observed in elliptical galaxies, and $R_{h,IR}$ is even larger. When the IR luminosity is as large as seen in the SCUBA observations (Pope et al. 2006), we predict that the characteristic sizes will be of the order of $\sim 10^{2.5}$ pc.

An important quantity associated with the time evolution of the various luminosities is their *duty cycle*. As in CO01 for a given luminosity $L(t)$, we define the associated duty cycle[6] over a period of time Δt as

$$f_{\rm duty} \equiv \frac{\left[\int_{t-\Delta t}^{t} L(t')\, dt'\right]^2}{\Delta t \int_{t-\Delta t}^{t} L^2(t')\, dt'}. \qquad (61)$$

[6] Defined in this way $f_{\rm duty}$ would be the fraction of the time a system would be in a high-luminosity state, L_h, and $1 - f_{\rm duty}$ would be the fraction of the time it spent in a low-luminosity state L_l, if it were to oscillate between these two states and $L_l/L_h \ll 1$.

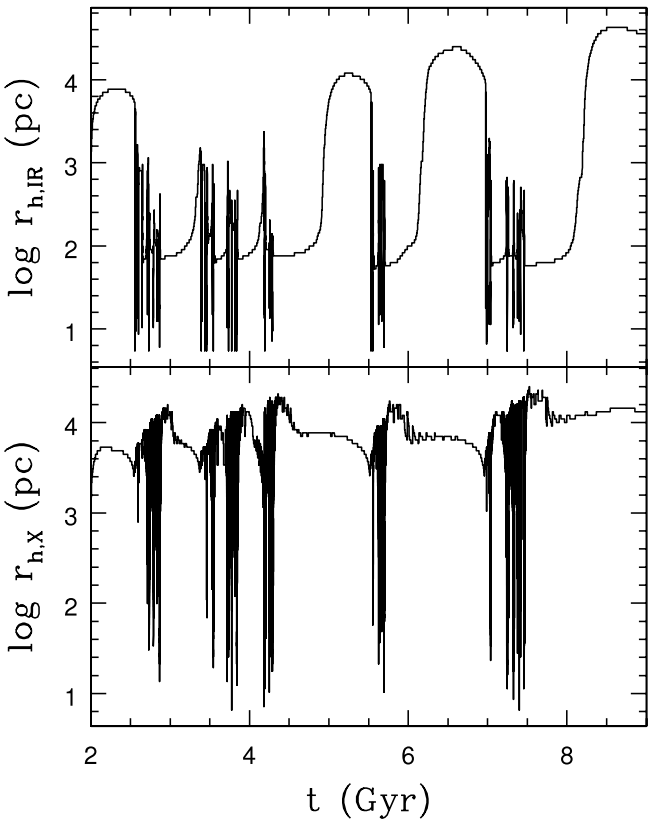

FIG. 4.—Time evolution of the (volume) half-light radius of the X-ray ISM luminosity (*bottom*) and IR luminosity (*top*) during the bursting phases. Small radii correspond to the high-luminosity peaks, and the predicted SCUBA-like sources should be of linear size $\sim 10^{2.5}$ pc.

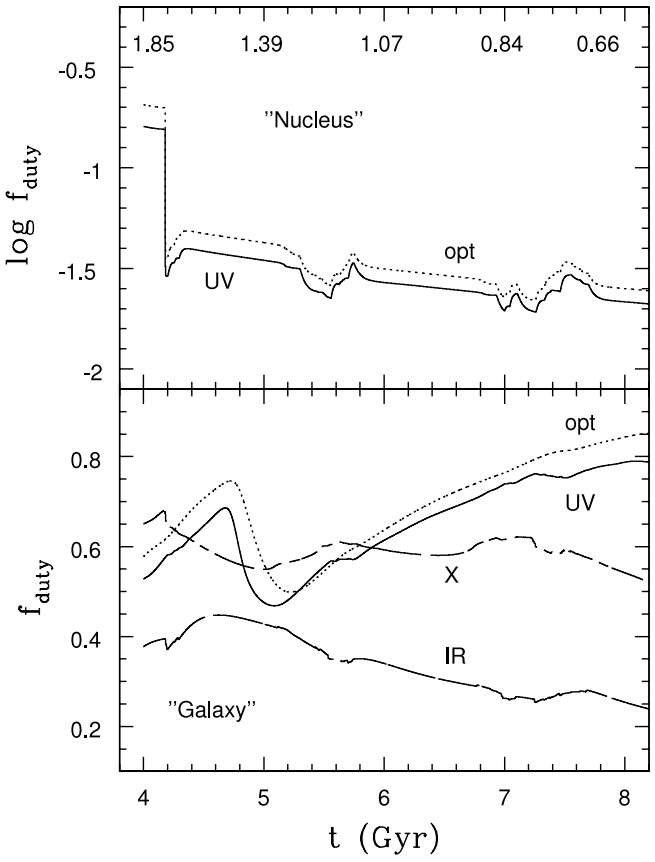

FIG. 5.—Time evolution of duty cycles as computed from eq. (61), with a time window $\Delta t = t/2$. *Top*: Duty cycle of $L^{\rm eff}_{\rm BH,UV}$ (*solid line*) and $L^{\rm eff}_{\rm BH,opt}$ (*dotted line*); the top axis shows the corresponding redshift (e.g., Spergel et al. 2007). We see that these systems would be observed from afar in the (rest frame) optical or UV as quasars several percent of the time. *Bottom*: Duty cycle of the starburst $L^{\rm eff}_{\rm UV}$ (*solid line*) and $L^{\rm eff}_{\rm opt}$ (*dotted line*) of the ISM X-ray luminosity (computed in a volume excluding the inner 100 pc) and of the recycled IR luminosity $L_{\rm IR}$.

In Figure 5 we show the resulting values for a time-dependent temporal window $\Delta t = t/2$. In the top panel we show the (logarithmic) value for the effective optical and UV AGN luminosities (with negative peaks corresponding to values as low as 0.01 or less), while during the smooth accretion of the last few Gyr the values flatten to unity. In the bottom panel the duty cycles correspond to the starburst optical and UV luminosities and show larger and less fluctuating values $\gtrsim 0.5$, in agreement with observational results (see, e.g., Cimatti et al. 2002). In the same panel we also show the duty cycle of the X-ray ISM luminosity computed outside a sphere of radius 100 pc, so as to exclude the ISM luminosity fluctuations produced by direct AGN heating on the surrounding ISM. In other words, the X-ray duty cycle refers to the bulk of the galactic body and should give an indication of the expected fraction of significantly disturbed galaxies in coronal X-rays. Quite obviously, the derived values depend on the adopted sampling time interval Δt. For example, by fixing the sampling time to $\Delta = 100$ Myr, the values in the bottom panel are almost unchanged, while the AGN duty cycle becomes (during peaks of activity) as small as $\sim 10^{-3}$. This is consistent with the temporal substructure of the major bursts (see Fig. 2). At the opposite end, taking the entire time interval spanned by the simulation, the AGN duty cycle (in both UV and optical) is $\sim 10^{-2}$, the IR is ~ 0.2, while the starburst duty cycle is ~ 0.8 and that of the global ISM X-ray is ~ 0.4. We stress here that the duty cycles are computed by the code calculating the luminosity values at *each* time step, which is usually of the order of 1 yr or even less.

Duty cycles can also be defined in a different way. For example, in Table 1 we focus in particular on the estimated time fraction spent by the central SMBH shining at a given fraction of Eddington luminosity, also considering the obscured accretion phases. Overall, in the bursting phase ($1 \lesssim z \lesssim 3$), the duty cycle of the SMBH in its "on" phase is of order percents and is unobscured approximately one-third of the time. We found it interesting that these figures, obtained from hydrodynamical simulations, can be positively compared with observations (see, e.g., Gilli et al. 2007; Martinez-Sansigre & Rawlings 2007).

3.2. *Mass Budgets*

In Figure 6 we show the time evolution of some of the relevant mass budgets of the model, as both time-integrated properties and instantaneous rates. At the end of the simulation the total ISM mass in the galaxy is $\sim 5 \times 10^8\ M_\odot$, while the SMBH mass increased by $2.5 \times 10^8\ M_\odot$, thus reaching a final mass of $\sim 7 \times 10^8\ M_\odot$: a model with a smaller initial SMBH mass would accrete less, thus maintaining the Magorrian relation even better. The SMBH mass accretion rate strongly oscillates as a consequence of radiative feedback, with peaks of the order of $10\ M_\odot\ {\rm yr}^{-1}$ (or more), while during the final, hot accretion phase the almost stationary accretion is $\lesssim 10^{-4}\ M_\odot\ {\rm yr}^{-1}$: this value is close to the estimates obtained for the nuclei of nearby galaxies (Pellegrini 2005). Note that in the last 6 Gyr the SMBH virtually stops its growth, while the ISM mass first increased due to the high mass return rate of the evolving stellar population and then decreased due to the global galactic wind induced by SNe Ia. During the

TABLE 1
TIME DISTRIBUTION OF EDDINGTON RATIOS

L_{BH}/L_{Edd} (1)	F_{ON} (%) (2)	$\Delta t_{obsc}/\Delta t_{ON}$ (%) (3)	F_{QSO} (%) (4)
>0.100	0.09	80	0.018
>0.030	1.51	94	0.096
>0.010	9.78	48	5.1
>0.003	22.48	36	14.4
>0.001	28.61	32	19.5

NOTES.—Col. (1): Adopted criterion to quantify the fraction of the time spent in the high-luminosity states of accretion, in terms of the emitted SMBH bolometric luminosity and the current Eddington luminosity. Col. (2): Time percentage (calculated over the model bursting period) $F_{ON} \equiv \Delta t_{ON}/\Delta t_{bursting}$, with $\Delta t_{bursting} = 5.5$ Gyr (see Fig. 1). Col. (3): Time percentage of obscuration (more than 2 mag in the rest-frame UV) calculated from the ratio $L^{eff}_{BH,UV}/0.2L_{BH}$ over the time interval Δt_{ON}. Col. (4): $F_{QSO} \equiv F_{ON} \times (1 - \text{col. [3]})$ gives the fraction of the bursting period during which there is less than 2 mag of obscuration in the rest-frame UV or less than 1.2 mag of obscuration in the rest-frame optical. This corresponds roughly to X-ray obscuration of $\approx 10^{22}$ atoms cm^{-2}.

entire model evolution, $\gtrsim 10^{10.5}\ M_\odot$ of recycled gas has been added to the ISM from stellar mass losses. Approximately $2.1 \times 10^{10}\ M_\odot$ has been expelled as a galactic wind, while $\sim 1.4 \times 10^{10}\ M_\odot$ has been transformed into new stars, so that only 0.7% of the recycled gas has been accreted onto the central SMBH, and the central paradox of the mass budget is automatically resolved.

In the present simulation, approximately twice of the total mass accreted onto the central SMBH is expelled as a disk wind, while the final mass of the disk, in stellar remnants, sums up to $m_{rem} \sim 2.8 \times 10^5\ M_\odot$. It is important to stress that an identical model without SMBH feedback (i.e., $\epsilon = 0$ in eq. [33]), but with the same star formation treatment of the model described in this paper, produced an SMBH of final mass $\gtrsim 10^{10}\ M_\odot$, while the total mass in new stars was reduced to $\sim 3 \times 10^9\ M_\odot$. In addition, this "ad hoc" model does not present fluctuations in the starburst and ISM X-ray luminosities, thus showing the vital importance of SMBH feedback in the overall results. Tests of numerical convergence were performed to determine the extent to which the results quoted in this paper would be altered as one increased the spatial and temporal resolution. To this end we reduced the grid

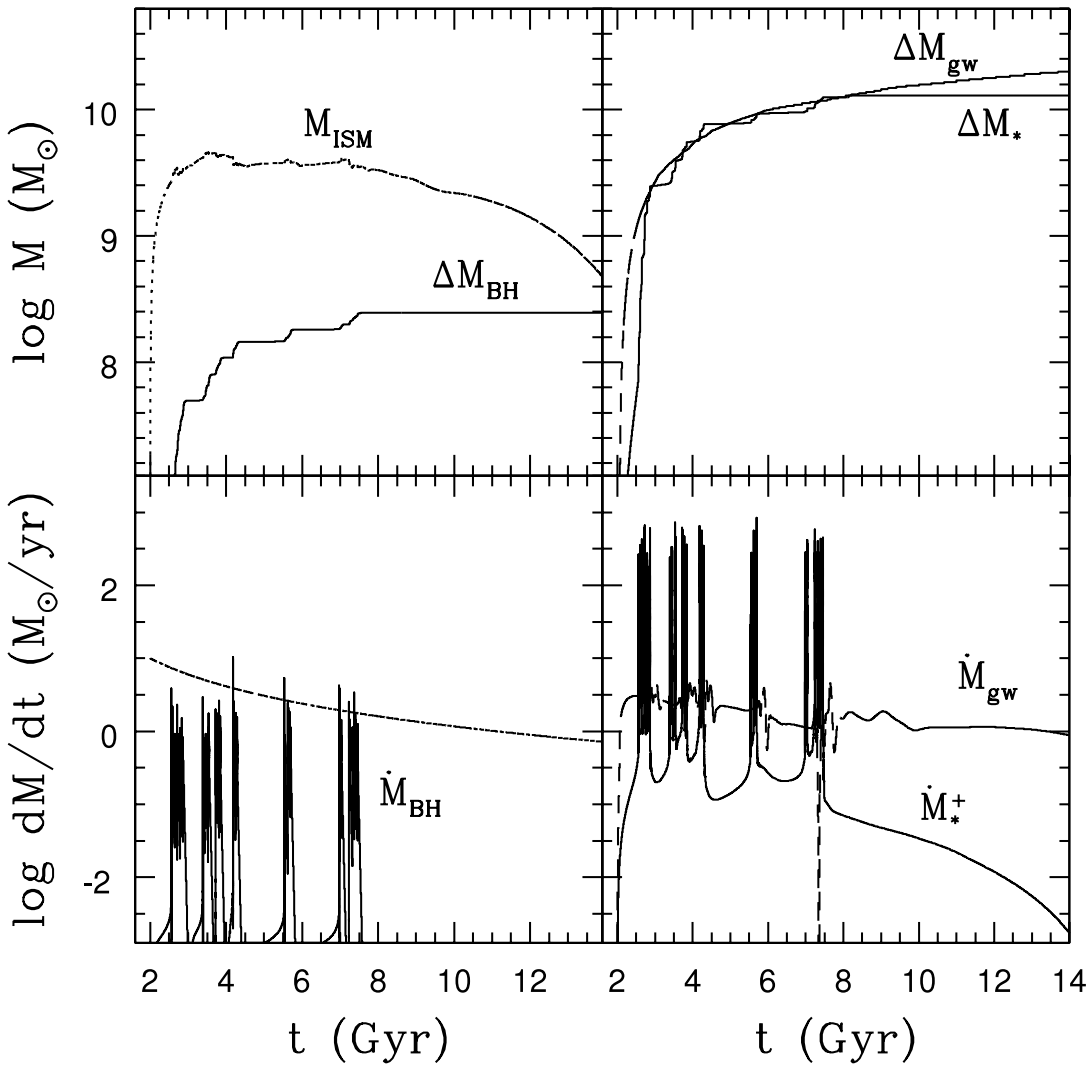

FIG. 6.—Mass budget evolution. *Top left*: Total hot gas mass in the galaxy (within $10R_e$, M_{ISM}; *dotted line*), and accreted mass on the central SMBH (ΔM_{BH}). *Top right*: Mass lost as a galactic wind at $10R_e$ (ΔM_{gw}; *dashed line*), and total mass of new stars (ΔM_*) formed according to eq. (15). *Bottom left*: Mass return rate from the evolving stellar population (as given by volume integral of eq. [13]; *dotted line*), and mass accretion rate on the central SMBH ($\dot{M}_{BH}$, eq. [26]). *Bottom right*: Galactic wind mass-loss rate at $10R_e$ ($\dot{M}_{gw}$; *dashed line*) and instantaneous, volume-integrated star formation rate. Note that for $t > 8$ Gyr the mass lost as a galactic wind is almost coincident with the mass input from evolving stars.

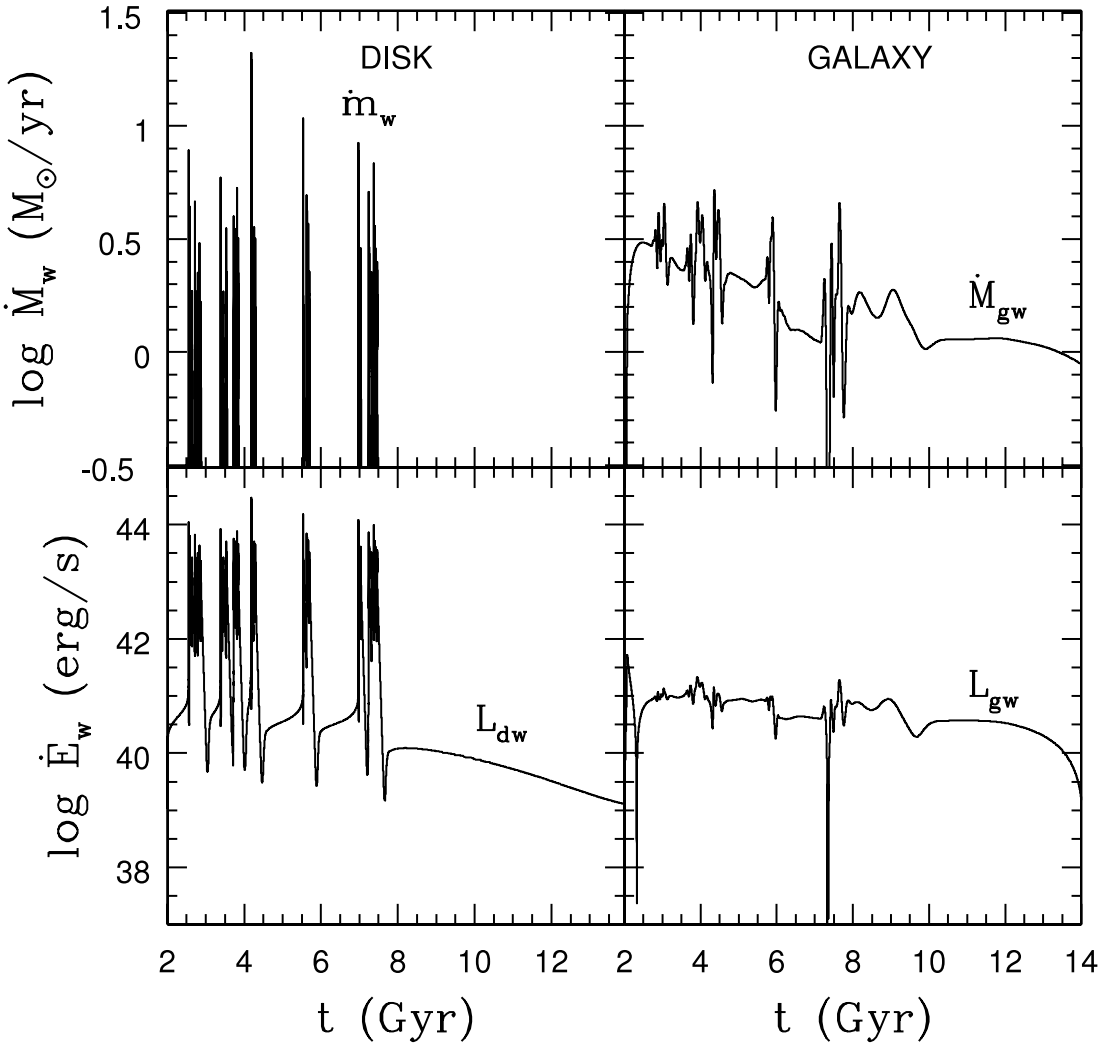

FIG. 7.—*Top*: Temporal evolution of the disk wind mass rate (eq. [32]; *left*) and the galactic wind mass rate computed at $10R_e$, $\dot{M}_{\rm gw} \equiv 4\pi(10R_e)^2\rho(10R_e)v(10R_e)$ (*right*). *Bottom*: Corresponding mechanical luminosities, i.e., the kinetic energy that would be injected from the disk in the galaxy ISM ($L_{\rm dw}$), and by the galaxy in the ICM, $L_{\rm gw} \equiv \dot{M}_{\rm gw}(10R_e)v^2(10R_e)/2$.

spacing by a factor of 1.5 and then a factor of 2.0. Almost all results changed at the level of a few percent or less (with the numerical uncertainty thus far below the level of the uncertainty in the physical modeling). The largest change found in the highest resolution run was in the growth of the central SMBH mass, with this growth being reduced by $\sim$14%. This is in the direction to make the final results conform more closely to the Magorrian relation with regard to $\Delta M_{\rm BH}/\Delta M_*$ (see Fig. 6).

Two important quantities associated with the mass budget of the model are the mechanical (nonrelativistic) wind luminosity of the disk, as given by equation (34), and the mechanical luminosity of the galaxy, i.e., the kinetic energy carried away by the global galactic wind (Figure 7, *bottom panels*; the corresponding mass rates are shown in the top panels). Time integration of these two mechanical luminosities over the entire model evolution revealed that the disk wind would deposit $\sim 2.2 \times 10^{59}$ ergs in the galaxy ISM, while the galactic wind would inject in the ICM $\sim 1.3 \times 10^{58}$ ergs.

The star formation rate during the periods of feedback-dominated accretion oscillates from 0.1 up to several hundred (with peaks near 10^3) solar masses per year, while it drops monotonically from 10^{-1} to $\lesssim 10^{-3}\ M_\odot\ {\rm yr}^{-1}$ in the last 6 Gyr of quiescent accretion (see Fig. 6). As already mentioned above, these violent star formation episodes (with SMBH accretion to star formation mass ratios $\sim 10^{-2}$ or less) are induced by accretion feedback[7] and are spatially limited to the central 10–100 pc; thus, the bulk of gas flowing to the center is consumed in the starburst. These findings are nicely supported by recent observations (see, e.g., § 5 in Lauer et al. 2005; see also Davies et al. 2007). Note that the "age" effect of the new stars on the global stellar population of the galaxy is small, as the new mass is only 3% of the original stellar mass, and it is virtually accumulated during the first few Gyr (see Fig. 6), so that the mass-weighted age of the final model is of the order of 12 Gyr. The half-mass radius of the final stellar distribution (without considering adiabatic contraction, nor the reduction of the stellar mass distribution due to galactic winds; see § 4) contracts by $\sim$16%, just due to the addition of the new stars in the central regions of the galaxy. This is made apparent in Figure 8, where we show the final spatial density profile of the system, together with its projection and the best fit obtained with the Sérsic (1968) law

$$\Sigma(R) = \Sigma_0 e^{-b(m)(R/R_e)^{1/m}}, \tag{62}$$

[7] However, bursting star formation is not necessarily associated with AGN feedback (see, e.g., Krügel & Tutukov 1993).

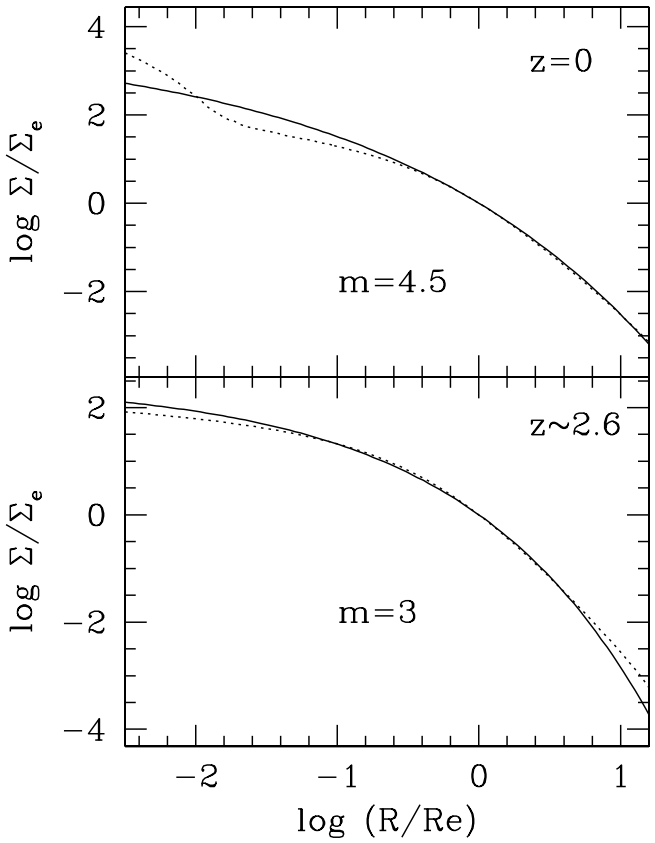

FIG. 8.—Dotted lines are the projected surface density of the model shortly after the beginning of the simulation ($t = 2.5$ Gyr, $z \sim 2.6$; *bottom*) and at $t = 13.5$ Gyr ($z = 0$; *top*), normalized to the surface density at the effective radius. The relation between age and redshift holds for standard cosmology (e.g., Spergel et al. 2007). Solid lines are the best-fit Sérsic law. The effective radius contracted from ~9.2 to ~8.4 kpc, while the surface density Σ_e increased from $\sim 3 \times 10^{22}$ to $\sim 3.6 \times 10^{22}$ protons cm^{-2}.

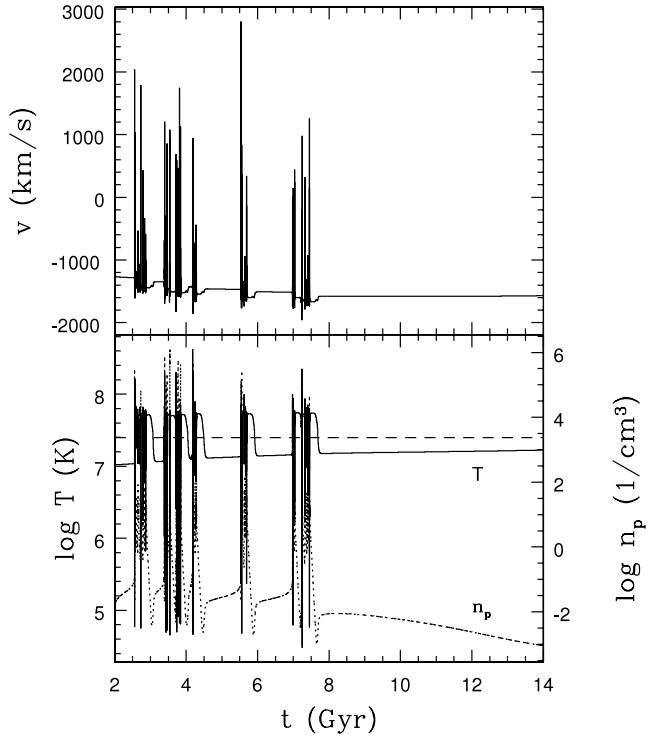

FIG. 9.—*Top*: Gas velocity at 5 pc from the SMBH. Note how the SMBH growth affects the lower envelope of velocity values. *Bottom*: Gas number density (*dotted line*; scale on the right axis) and temperature at 5 pc from the SMBH (*solid line*). Low-temperature, high-density phases end when accretion luminosity $L_{\rm BH}$ increases sharply, heating the ambient gas to a high-temperature, low-density state. The horizontal dashed line is the model Compton temperature $T_{\rm X} = 2.5 \times 10^7$ K.

where $b(m) = 2m - 1/3 + 4/(405m)$ (Ciotti & Bertin 1999). As expected, the profiles show an increase of the best-fit Sérsic parameter m, due to the mass accumulation in the central regions. Remarkably, the final value of m is within the range of values commonly observed in ellipticals: however, in the final model we note the presence of a central (~30 pc) nucleus originated by star formation that stays above the best-fit profile, similar to the light spikes characterizing "nucleated" galaxies (see, e.g., Graham & Driver 2005; Coté et al. 2006).

3.3. *Hydrodynamics*

In Figure 9 we show the temperature and density in the central regions of the model: note how the SMBH bursts heat the central gas, causing the density to drop, and launching gas at positive velocities of the order of thousands of kilometers per second (this can be better appreciated in Fig. 10, where we show a time blowup of the first two SMBH feedback events). The Compton temperature is the horizontal dashed line, and during the bursts the local gas is heated above this limit.

As was already found in CO01, the galaxy cooling catastrophe starts with the formation of a *cold shell* placed around the galaxy core radius; however, in the present models (as in those explored by Pellegrini & Ciotti 1998), the cooling catastrophe happens at significantly earlier times than in CO01 models, due both to the higher central stellar density and to the different time dependence and amount of SN Ia explosions. The three main evolutionary phases of the model are summarized in Figures 11–14. In particular,

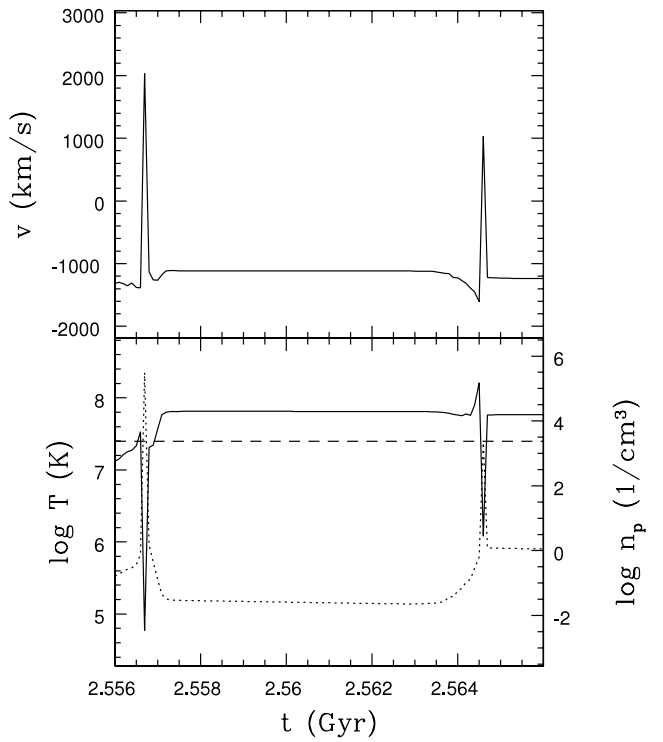

FIG. 10.—Time expansion of the first two feedback events of the initial major burst in Fig. 9 (whose total time extent is ~400 Myr) at time resolution 10^5 yr; the horizontal dashed line is the model Compton temperature. The complementary behavior of ρ and T is apparent.

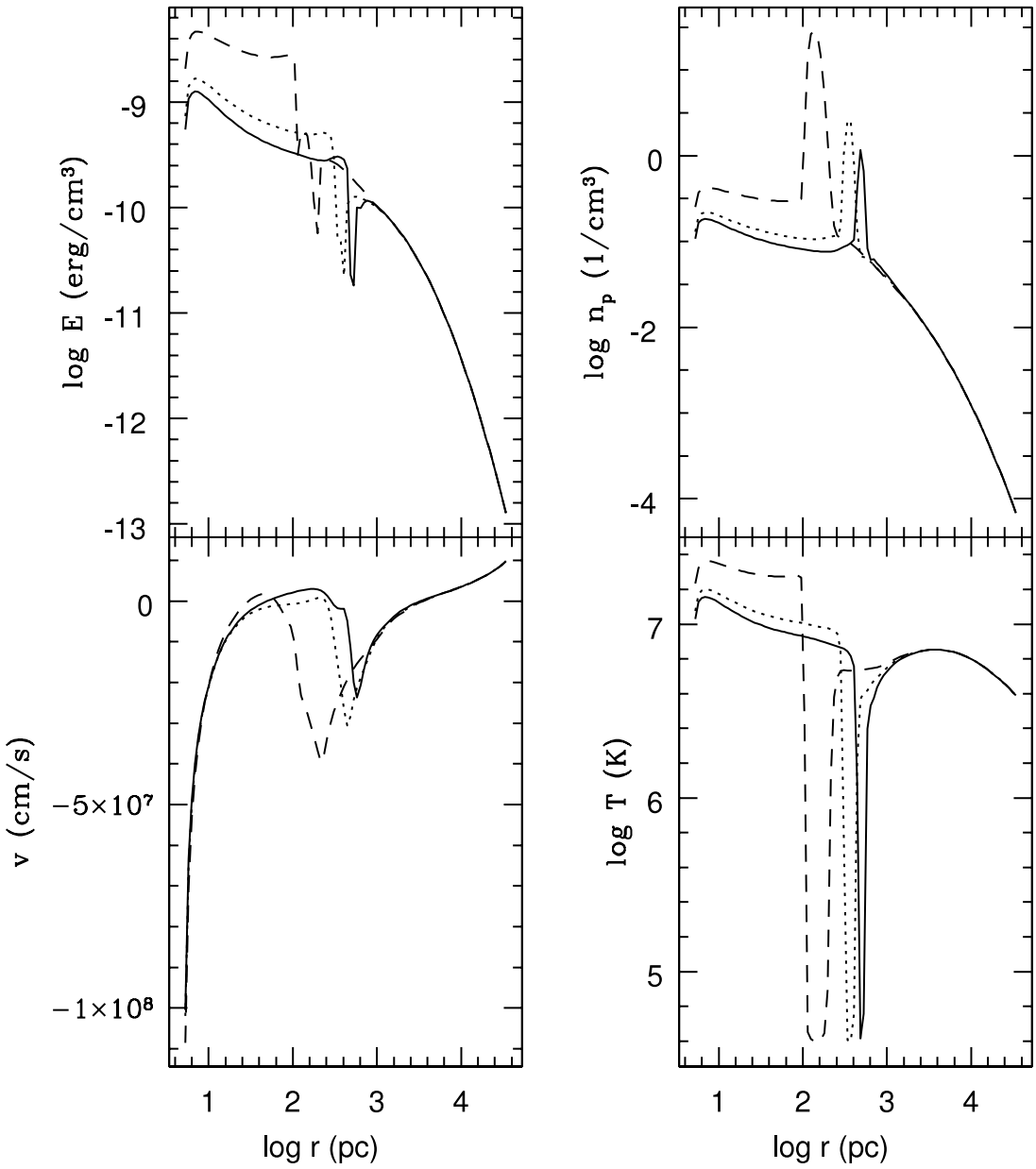

FIG. 11.—Hydrodynamical quantities of the model immediately before the onset of the bursting phase (2.554 Gyr), separated by 1 Myr (in order, solid, dotted, and dashed lines). The cold shell is falling toward the galactic center.

in Figure 11 one can observe (with time separation of 1 Myr) the evolution of the first cold shell falling to the galactic center, while in Figure 12 (*dashed line*) the expanding material due to the first burst (with velocities of the order of several hundred kilometers per second) is clearly visible. A particularly important feature can be noticed in Figure 13, where a new cold and dense shell of gas is formed as a consequence of the shock wave produced by the burst. This shell moves (slowly) outward and then starts to fall back at the center; in the shell, the star formation rate reaches values of $\sim 10^{-8}\ M_{\odot}\ \mathrm{yr}^{-1}\ \mathrm{pc}^{-3}$. We stress that this shell is of a different origin compared to the first, and it is possibly Rayleigh-Taylor unstable. This cycle of shell formation, central burst, and expanding phase repeats during the entire bursting evolution, along the lines described in detail in CO01. Finally, when the specific SN Ia heating becomes dominant over the decline of fresh mass input from evolving stars, the galaxy hosts a wind, the accretion becomes stationary without oscillations, and the central SMBH is radiating at $\sim 10^{-5} L_{\mathrm{Edd}}$ (Hopkins et al. 2006b). The hydrodynamical quantities (separated now by a time interval of 0.5 Gyr) are shown in Figure 14.

4. CONCLUSIONS AND DISCUSSION

In this paper we have addressed the effects of radiative feedback on the gas flows in elliptical galaxies. The investigation is in the line of previous exploratory papers (CO97; CO01; OC05), but now the input physics and the galaxy models have been substantially improved. We briefly recall here the main points on which our framework is based. First of all, it is obvious that the recycled gas from dying stars is an important source of fuel for the central SMBH, *even in the absence of external phenomena such as galaxy merging*, which are often advocated as the way to induce QSO activity. It is also obvious that the recycled gas, arising from stars in the inner several kiloparsecs of the galaxy (assumed a giant elliptical), will necessarily drive a classical radiative instability and a collapse toward the center of metal-rich gas. As a consequence, a starburst must occur and also the

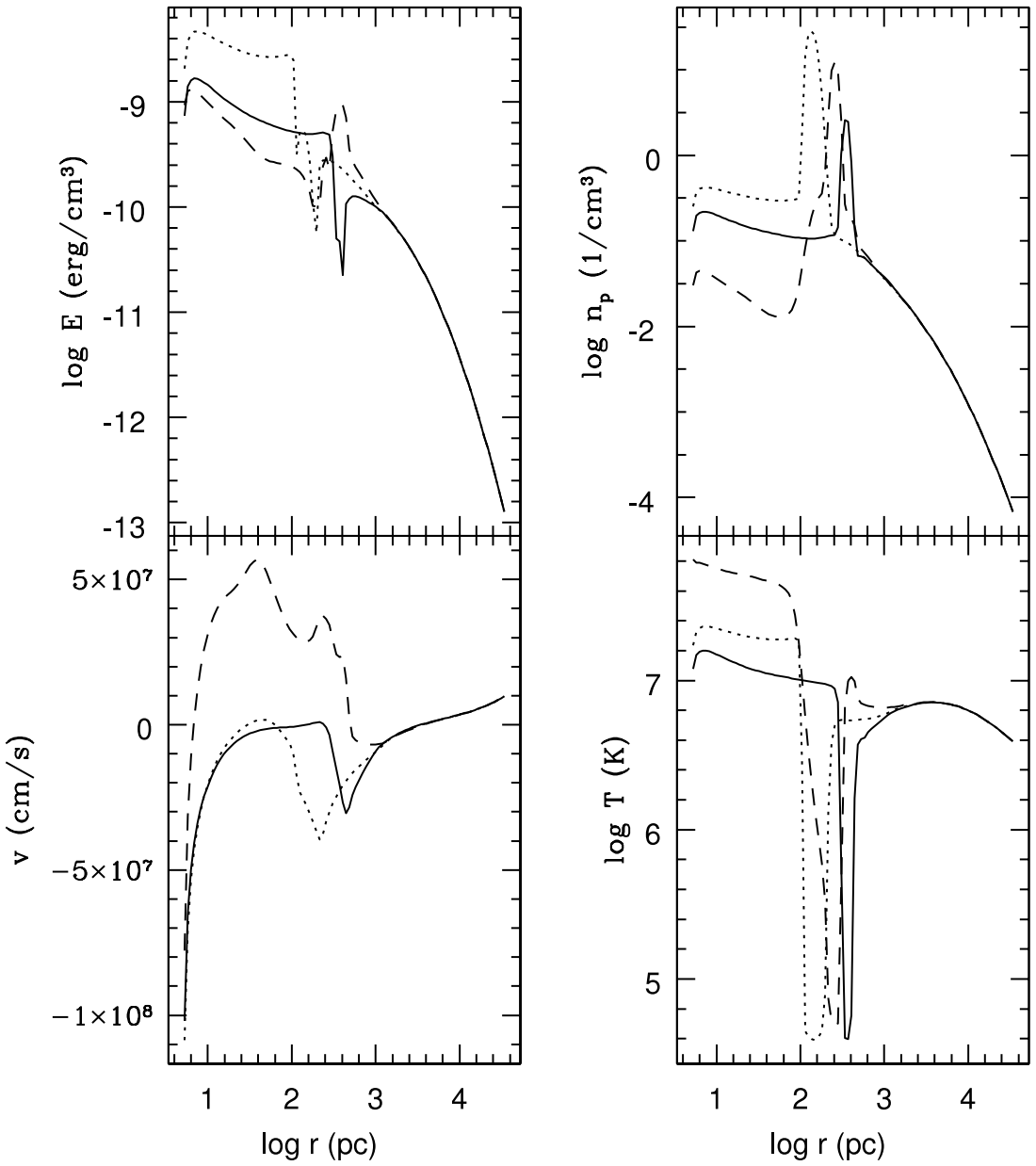

FIG. 12.—Cold shell reached the center, and a shock wave is moving outward (*dashed lines*; note the positive velocities). Time interval is 1 Myr (in order, solid, dotted, and dashed lines), and the first two snapshots are the last two snapshots in Fig. 11.

central SMBH must be fed. The details of how much is accreted on the central SMBH versus consumed in stars versus ejected from the center by energy input from the starburst and AGN are uncertain. But order-of-magnitude estimates would have the bulk going into stars or blown out as a galactic wind, with a small amount going into the central SMBH. In addition, since at the end of a major outburst a hot bubble remains at the center, both processes shut themselves off, and it will take a cooling time for the cycle to repeat. In other words, relaxation oscillations are to be expected, but their detailed character is uncertain. Finally, order-of-magnitude estimates would indicate that during the bursting phase the center would be optically thick to dust, so one would observe a largely obscured starburst and largely obscured AGN with most radiation in the far-IR; as gas gets consumed, the central sources become visible. Much of the AGN output occurs during obscured phases, then there is a brief interval when one sees a "normal" quasar, and finally one would see a low X-ray luminosity and E+A spectrum galaxy, with A dominating in the central several hundred parsecs for 10^7–10^8 yr.

The present paper attempts to illustrate the expectations described above. Overall, we have confirmed that radiative feedback from a central SMBH has dramatic effects on galaxy evolution and on the mass growth of the central SMBH itself, and we find that much of the recycled gas falling toward the galactic center during the accretion events is consumed in central starbursts with a small fraction (of the order of 1% or less) accreted onto the central SMBH. In particular, in the presented model approximately half of the recycled mass from evolving stars is expelled in the ICM, while the remaining fraction is consumed in central starbursts. Thus, the central starburst is an important component in the physical modeling, since it regulates the amount of gas available to be accreted onto the central SMBH: without allowing for the (AGN feedback induced) central star formation the SMBH would grow to be far more massive than seen in real galaxies. While the details predicted by our simulations are uncertain,

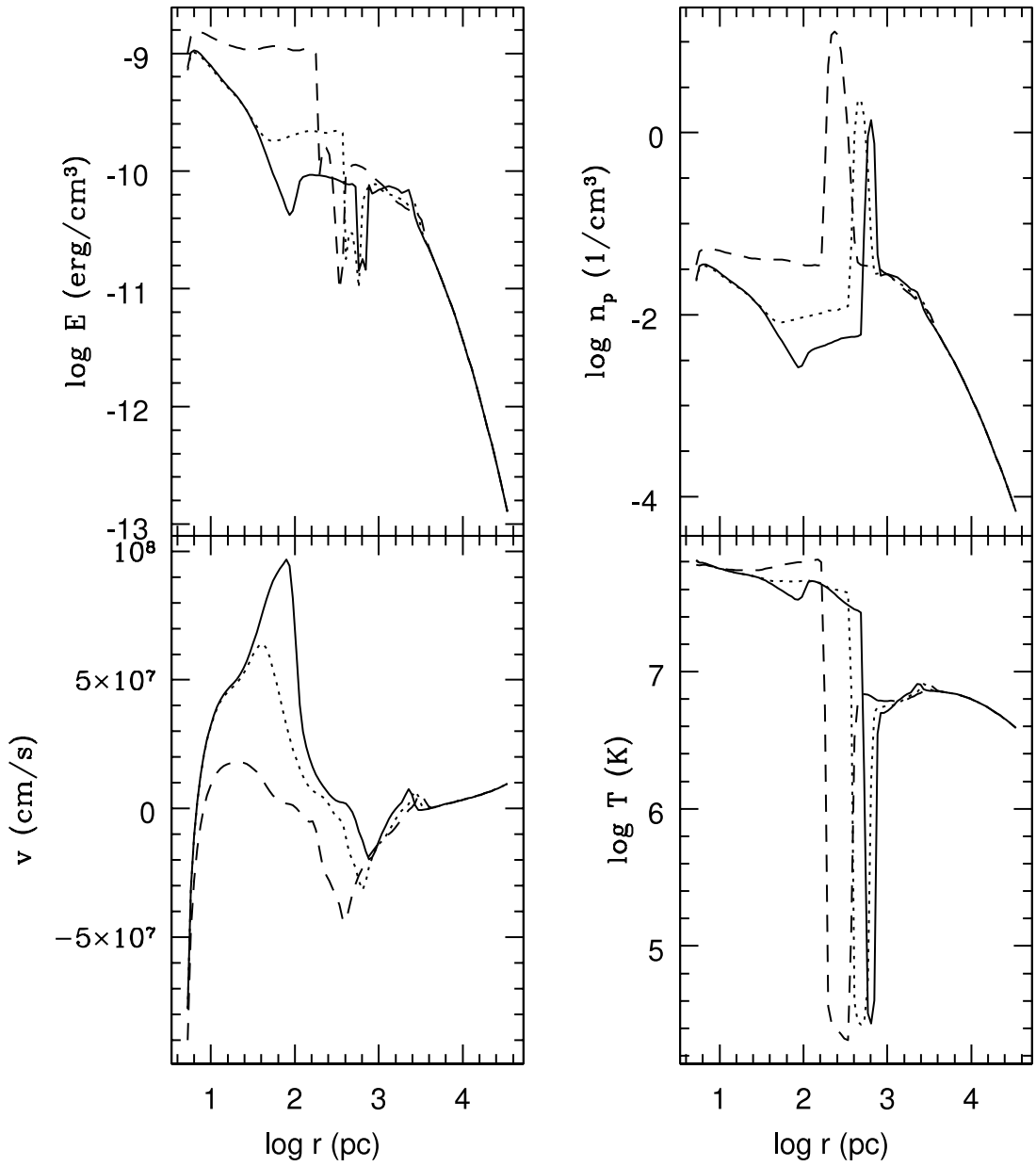

FIG. 13.—Expanding flow produced a new cold shell, which starts to fall to the galactic center. Time interval is 1 Myr (in order, solid, dotted, and dashed lines), while the time is now 2.561 Gyr.

we do not see how this sequence can be avoided in its qualitative features. The input is standard physics plus the known radiative output from the SMBH and stars. Other processes that we do not include in the present code may also be important. For example, the mechanical energy from the AGN and cosmic rays from the supernova remnant in the starburst are surely important (see, e.g., Di Matteo et al. 2005), but we deliberately excluded them from the present investigation to better assess the importance of radiative feedback (as both heating and radiative pressure).

The main results of our simulations, also considering all the simplifications in the treatment of physics and of the geometry of the code, nicely support the scenario depicted above. In particular, *we showed how complicated the evolution of an isolated galaxy, subject to internal evolution only, can be* (see, e.g., Pierce et al. 2007). From the observational point of view, we find that evidence for starbursts should be common when looking at elliptical galaxies, with the fraction showing an E+A spectrum increasing with redshift (with preliminary evidence for high metallicity in the new stellar spectra). Also, signs of star formation in high-z objects such as those detected in UV (*GALEX*) and IR (*Spitzer*), or accompanying AGNs (X-ray), should be common (see, e.g., Yan et al. 2006; Nesvadba et al. 2006, Simoes Lopes et al. 2007), with IR luminosity peaks of $\sim 10^{46}$ ergs s^{-1}. Due to the observational relevance of these predictions, a more accurate modelization of the expected IR model properties would be a natural extension of the present work (e.g., Chakrabarti et al. 2007).

We note that there is increasing evidence in the local universe of hot gas disturbances on various galactic scales, likely the resultant from recent nuclear activity (e.g., Forman et al. 2007; McNamara & Nulsen 2007). For example, *Chandra* revealed two symmetric armlike features across the center of NGC 4636 (Jones et al. 2002; O'Sullivan et al. 2005), accompanied by a temperature increase with respect to the surrounding hot ISM; they were related to shock heating of the ISM, caused by a recent nuclear outburst. Other evidences include a hot filament in the nuclear regions of NGC 821 and NGC 3377 (Fabbiano et al.

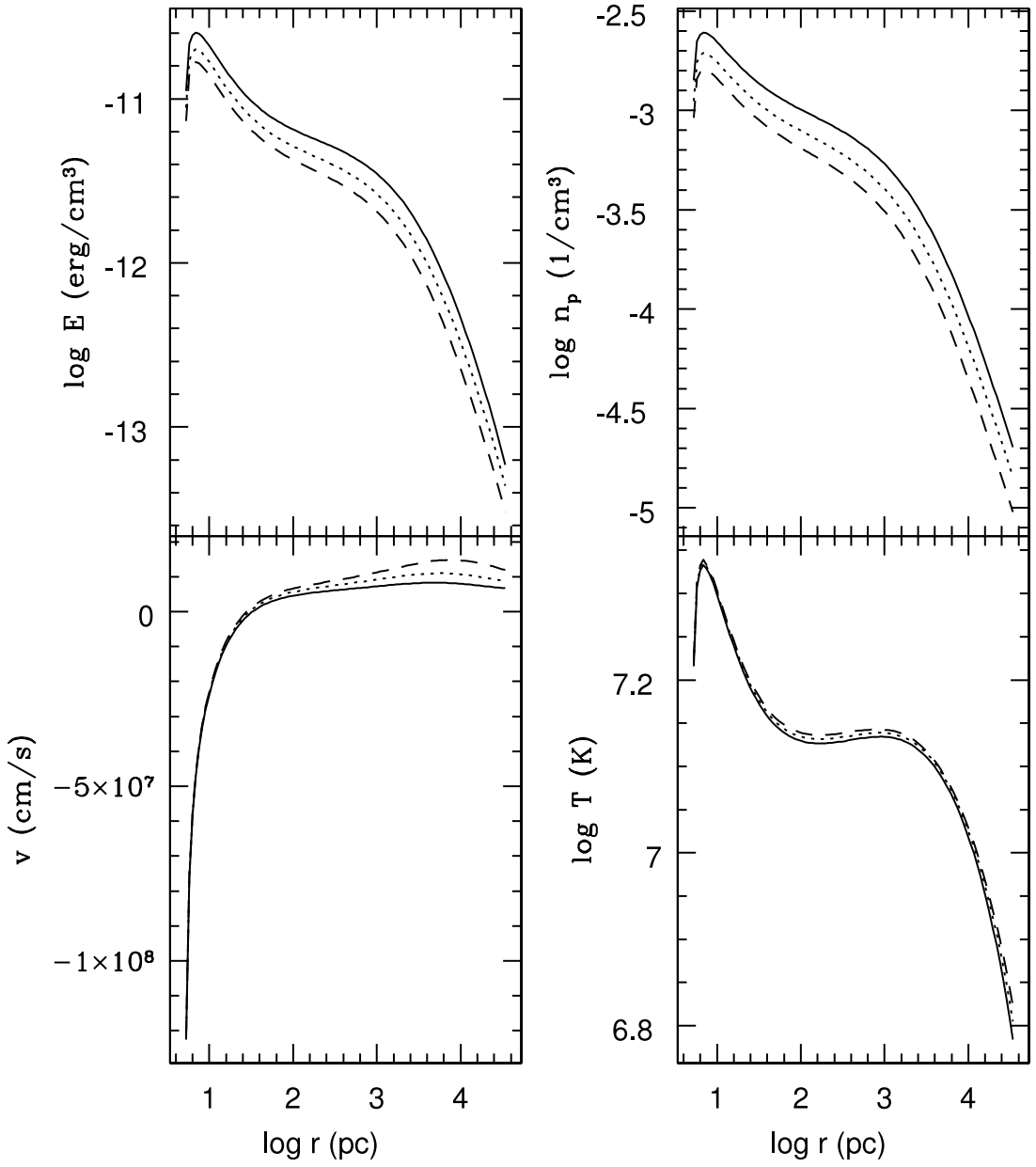

FIG. 14.—Hydrodynamical quantities of the model at the end of the simulation, separated by 0.5 Gyr (in order, solid, dotted, and dashed lines). The galaxy is in the low-luminosity, high-temperature, and low-density stationary accretion phase in the inner parts, and in its outer parts a $\sim$100–200 km s^{-1} wind is carrying out most of the late recycled gas.

2004; Soria et al. 2006); a "bar" feature, presumably due to a shock, at the center of NGC 4649 (Randall et al. 2004); a nuclear outflow in NGC 4438 (Machacek et al. 2004); and, finally, an unusual temperature profile present in NGC 3411 (O'Sullivan et al. 2007).

In this paper we presented just one out of many models, to illustrate in detail the global behavior of a typical solution. Of course, the present work suffers from some weak points, as follows: (1) We neglected the modifications of the galaxy gravity field and velocity dispersion profile due to the stellar mass losses, galactic wind, and star formation (deepening the central potential). (2) The new stars are placed in the galaxy where they form. (3) The additional effect of mechanical feedback was not taken into account (see, e.g., Begelman & Ruszkowski 2005). (4) Finally, the simulations are spherically symmetric, so that Rayleigh-Taylor unstable configurations of the ISM, as well as the formation of an accretion disk, cannot be followed.

Several lines of investigation will be studied in future papers, in order to better test the results and to address specific points only mentioned here. For example, it is natural to study in detail the properties expected for the starburst population (such as spatial distribution, spectral properties, etc.) and the X-ray properties of the perturbed ISM, as a function of the combined effect of SNe Ia and central feedback. Other obvious issues to be addressed are the effects of environment, as for a cD galaxy in a cluster; this study will also probe the impact of photoionization plus Compton heating on the ICM (extending the preliminary investigation of Ciotti et al. 2004; see also Pope et al. 2007). Also, the modifications of the galaxy inner structure and dynamics due to star formation are important, in particular for the expected evolution of the Magorrian and $M_{\rm BH}$-σ relations. A most relevant extension of the present work would also be the study of radiative feedback by using two-dimensional codes, in order to follow the evolution of unstable features found here, such as the cold-shell phase, and

to properly describe axisymmetric accretion in the optically thick regime (e.g., Krolik 2007; Proga 2007). We finally mention another observational riddle that could be addressed with the present models, i.e., that of the apparent "underluminosity" of SMBHs in the local universe (see, e.g., Fabian & Canizares 1988; Pellegrini 2005). The present models could also be used in a different way. In fact, when addressing galaxy evolution over cosmological times, two main effects have not been considered in the present treatment, namely, galaxy formation itself and the successive cosmological infall and merging events (e.g., Hopkins & Hernquist 2006; Micic et al. 2007). These aspects of evolution are usually considered in cosmological simulations (see, e.g., Springel et al. 2005; Naab et al. 2007 and references therein), and so it would be interesting to add at the center of galaxies in those simulations the treatment of feedback physics described here.

We thank Annibale D'Ercole, Bruce Draine, Martin Elvis, Roberto Gilli, Jeremy Goodman, Avi Loeb, Eve Ostriker, Silvia Pellegrini, and Todd Thompson for useful discussions and the anonymous referee for important remarks. L. C. was partially supported by the grant CoFin2004 by Italian MIUR.

APPENDIX

NUMERICAL EVALUATION OF LAG INTEGRALS

Time lag integrals often appear in the code. It is possible to compute them numerically without much use of computer memory.[8] In fact, let $f(t)$ be a given function of time, and let

$$F(t) = \int_0^t f(t')e^{-(t-t')/\tau_{\rm lag}}\,dt' \tag{A1}$$

be the quantity to be determined. It is easy to prove that for $t_i \le t$ the exact identity

$$F(t) = F(t_i)e^{-(t-t_i)/\tau_{\rm lag}} + \int_{t_i}^t f(t')e^{-(t-t')/\tau_{\rm lag}}\,dt' \tag{A2}$$

holds, so that only the storage of values $F(t_i)$ and $f(t_i)$ is necessary to evaluate $F(t_{i+1})$. Note that equation (A1) is the solution of the differential equation

$$\frac{dF}{dt} = f(t) - \frac{F(t)}{\tau_{\rm lag}}, \tag{A3}$$

and this leads to an alternative way to compute $F(t)$ by using (for instance) a finite-difference integration scheme. In the integration of the hydrodynamical equations the evaluation of the quantity $\Delta F = \int_{t_i}^{t_{i+1}} F(t)\,dt$ over a time step is also often required. From equations (A1) and (A2), simple algebra proves the exact relation

$$\Delta F = \tau_{\rm lag}[F(t_i) - F(t_{i+1})] + \tau_{\rm lag}\int_{t_i}^{t_{i+1}} f(t')\,dt'. \tag{A4}$$

In the code, the function f is defined as the linear interpolation between the initial and final time over the time step, so that the integrals given by equations (A2) and (A4) can be explicitly calculated with negligible computer time.

[8] Note that in CO01 the exponential factors in front of the integral in eq. (B2) and inside the integral in eq. (B3) are two typos.

REFERENCES

Begelman, M. C., & Nath, B. B. 2005, MNRAS, 361, 1387
Begelman, M. C., & Ruszkowski, M. 2005, Philos. Trans. R. Soc. London A, 363, 655
Bertin, G., et al. 1994, A&A, 292, 381
Binney, J. 2001, in ASP Conf. Ser. 250, Particles and Fields in Radio Galaxies Conference, ed. R. A. Laing & K. M. Blundell (San Francisco: ASP), 481
Binney, J., & Tabor, G. 1995, MNRAS, 276, 663
Burkert, A., & Silk, J. 2001, ApJ, 554, L151
Cappellari, M., et al. 2006, MNRAS, 366, 1126
Cappellaro, E., Evans, R., & Turatto, M. 1999, A&A, 351, 459
Cavaliere, A., & Vittorini, V. 2002, ApJ, 570, 114
Cen, R., & Ostriker, J. P. 2006, ApJ, 650, 560
Chakrabarti, S., Cox, T. J., Hernquist, L., Hopkins, P. F., Robertson, B., & Di Matteo, T. 2007, ApJ, 658, 840
Chandrasekhar, S. 1960, Radiative Transfer (New York: Dover)
Churazov, E., Sazonov, S., Sunyaev, R., Forman, W., Jones, C., & Böhringer, H. 2005, MNRAS, 363, L91
Cimatti, A., et al. 2002, A&A, 381, L68
Ciotti, L. 1996, ApJ, 471, 68
Ciotti, L., & Bertin, G. 1999, A&A, 352, 447
Ciotti, L., D'Ercole, A., Pellegrini, S., & Renzini, A. 1991, ApJ, 376, 380 (C91)
Ciotti, L., Lanzoni, B., & Renzini, A. 1996, MNRAS, 282, 1
Ciotti, L., & Ostriker, J. P. 1997, ApJ, 487, L105 (CO97)
———. 2001, ApJ, 551, 131 (CO01)
Ciotti, L., Ostriker, J. P., & Pellegrini, 2004, in AIP Conf. Proc. 703, Plasmas in the Laboratory and in the Universe: New Insights and New Challenges, ed. G. Bertin, D. Farina, & R. Pozzoli (New York: AIP), 367
Ciotti, L., & Pellegrini, S. 1992, MNRAS, 255, 561
Coté, P., et al. 2006, ApJS, 165, 57
Cowie, L. L., Ostriker, J. P., & Stark, A. A. 1978, ApJ, 226, 1041
Croton, D. J., et al. 2006, MNRAS, 365, 11
Davies, R. I., Mueller Sánchez, F., Genzel, R., Tacconi, L., Hicks, E., Friedrich, S., & Sternberg, A. 2007, ApJ, submitted (arXiv: 0704.1374)
D'Ercole, A., Recchi, S., & Ciotti, L. 2000, ApJ, 533, 799
D'Ercole, A., Renzini, A., Ciotti, L., & Pellegrini, S. 1989, ApJ, 341, L9
Di Matteo, T., Springel, V., & Hernquist, L. 2005, Nature, 433, 604
Douglas, N. G., et al. 2007, ApJ, 664, 257
Dubinski, J., & Carlberg, R. G. 1991, ApJ, 378, 496
Elvis, M. 2006, Mem. Soc. Astron. Italiana, 77, 573
Fabbiano, G., Baldi, A., Pellegrini, S., Siemiginowska, A., Elvis, M., Zezas, A., & McDowell, J. 2004, ApJ, 616, 730
Faber, S. M., et al. 1997, AJ, 114, 1771

Fabian, A. C. 1999, MNRAS, 308, L39
Fabian, A. C., & Canizares, C. R. 1988, Nature, 333, 829
Fabian, A. C., Celotti, A., & Erlund, M. C. 2006, MNRAS, 373, L16
Fabian, A. C., Thomas, P. A., Fall, S. M., & White, R. E., III 1986, MNRAS, 221, 1049
Ferrarese, L., & Merritt, D. 2000, ApJ, 539, L9
Forman, W., et al. 2007, ApJ, in press (astro-ph/0604583)
Fukugita, M., Nakamura, O., Turner, E. L., Helmboldt, J., & Nichol, R. C. 2004, ApJ, 601, L127
Fukushige, T., & Makino, J. 1997, ApJ, 477, L9
Gebhardt, K., et al. 2000, ApJ, 539, L13
Gilli, R., Comastri, A., & Hasinger, G. 2007, A&A, 463, 79
Goodman, J., & Tan, J. C. 2004, ApJ, 608, 108
Graham, A. W., & Driver, S. P. 2005, Publ. Astron. Soc. Australia, 22, 118
Graham, A. W., Erwin, P., Caon, N., & Trujillo, I. 2003, Rev. Mex. AA Ser. Conf., 17, 196
Granato, G. L., De Zotti, G., Silva, L., Bressan, A., & Danese, L. 2004, ApJ, 600, 580
Greggio, L. 2005, A&A, 441, 1055
Haiman, Z., Ciotti, L., & Ostriker, J. P. 2004, ApJ, 606, 763
Hernquist, L. 1990, ApJ, 356, 359
Hopkins, P. F., & Hernquist, L. 2006, ApJS, 166, 1
Hopkins, P. F., Hernquist, L., Cox, T. J., Robertson, B., Di Matteo, T., & Springel, V. 2006a, ApJ, 639, 700
Hopkins, P. F., Narayan, R., & Hernquist, L. 2006b, ApJ, 643, 641
Humphrey, P. J., Buote, D. A., Gastaldello, F., Zappacosta, L., Bullock, J. S., Brighenti, F., & Mathews, W. G. 2006, ApJ, 646, 899
Imanishi, M., Dudley, C. C., Maiolino, R., Maloney, P. R., Nakagawa, T., & Risaliti, G. 2007, ApJS, 171, 72
Jaffe, W., Ford, H. C., O'Connell, R. W., van den Bosch, F. C., & Ferrarese, L. 1994, AJ, 108, 1567
Jones, C., Forman, W., Vikhlinin, A., Markevitch, M., David, L., Warmflash, A., Murray, S., & Nulsen, P. E. J. 2002, ApJ, 567, L115
Kawata, D., Cen, R., & Ho, L. C. 2007, ApJ, submitted (arXiv: 0706.0005)
King, A. R. 2003, ApJ, 596, L27
King, A. R., Pringle, J. E., & Livio, M. 2007, MNRAS, 376, 1740
King, I. R. 1972, ApJ, 174, L123
Krolik, J. H. 2007, ApJ, 661, 52
Krügel, E., & Tutukov, A. V. 1993, A&A, 275, 416
Lauer, T. R., et al. 2005, AJ, 129, 2138
Machacek, M. E., Jones, C., & Forman, W. R. 2004, ApJ, 610, 183
Magorrian, J., et al. 1998, AJ, 115, 2285
Mannucci, F., Della Valle, M., Panagia, N., Cappellaro, E., Cresci, G., Maiolino, R., Petrosian, A., & Turatto, M. 2005, A&A, 433, 807
Maraston, C. 2005, MNRAS, 362, 799
Martinez-Sansigre, A., & Rawlings, S. 2007, preprint (astro-ph/0701143)
Matteucci, F., Panagia, N., Pipino, A., Mannucci, F., Recchi, S., & Della Valle, M. 2006, MNRAS, 372, 265
McLure, R. J., & Dunlop, J. S. 2002, MNRAS, 331, 795
McNamara, B. R., & Nulsen, P. E. J. 2007, ARA&A, 45, 117
Micic, M., Holley-Bockelmann, Sigurdsson, S., & Abel, T. 2007, MNRAS, submitted (astro-ph/0703540)
Murray, N., Quataert, E., & Thompson, T. A. 2005, ApJ, 618, 569
Naab, T., Johansson, P. H., Ostriker, J. P., & Efstathiou, G. 2007, ApJ, 658, 710
Narayan, R., & Yi, I. 1994, ApJ, 428, L13
Navarro, J. F., Frenk, C. S., & White, S. D. M. 1997, ApJ, 490, 493
Nayakshin, S., Dehnen, W., Cuadra, J., & Genzel, R. 2006, MNRAS, 366, 1410
Nayakshin, S., & Sunyaev, R. 2005, MNRAS, 364, L23
Neill, J. D., et al. 2007, preprint (astro-ph/0701161)
Nesvadba, N. P. H., Lehnert, M. D., Eisenhauer, F., Gilbert, A., Tecza, M., & Abuter, R. 2006, ApJ, 650, 693
Nolan, L. A., Raychaudhury, S., & Kabán, A. 2007, MNRAS, 375, 381
Omma, H., Binney, J., Bryan, G., & Slyz, A. 2004, MNRAS, 348, 1105
Ostriker, J. P., & Ciotti, L. 2005, Philos. Trans. R. Soc. London A, 363, 667 (OC05)
Ostriker, J. P., Weaver, R., Yahil, A., & McCray, R. 1976, ApJ, 208, L61
O'Sullivan, E., Ponman, T. J., & Collins, R. S. 2003, MNRAS, 340, 1375
O'Sullivan, E., Vrtilek, J. M., Harris, D. E., & Ponman, T. J. 2007, ApJ, 658, 299
O'Sullivan, E., Vrtilek, J. M., & Kempner, J. C. 2005, ApJ, 624, L77
Pellegrini, S. 2005, ApJ, 624, 155
Pellegrini, S., & Ciotti, L. 1998, A&A, 333, 433
———. 2006, MNRAS, 370, 1797
Peterson, J. R., & Fabian, A. C. 2006, Phys. Rep., 427, 1
Pierce, C. M., et al. 2007, ApJ, 660, L19
Pope, A., et al. 2006, MNRAS, 370, 1185
Pope, E. C. D., Pavlosvski, G., Kaiser, C. R., & Fangohr, H. 2007, preprint (astro-ph/0702683)
Proga, D. 2007, ApJ, 661, 693
Randall, S. W., Sarazin, C. L., & Irwin, J. A. 2004, ApJ, 600, 729
Renzini, A., & Ciotti, L. 1993, ApJ, 416, L49
Renzini, A., Ciotti, L., D'Ercole, A., & Pellegrini, S. 1993, ApJ, 419, 52
Reuland, M., et al. 2007, AJ, 133, 2607
Riciputi, A. Lanzoni, B., Bonoli, S., & Ciotti, L. 2005, A&A, 443, 133
Roberts, M. S., Hogg, D. E., Bregman, J. N., Forman, W. R., & Jones, C. 1991, ApJS, 75, 751
Rodighiero, G., et al. 2007, MNRAS, 376, 416
Russell, P. A., Ponman, T. J., & Sanderson, A. J. R. 2007, MNRAS, 378, 1217
Saglia, R. P., et al. 1993, ApJ, 403, 567
Sazonov, S. Yu., Ostriker, J. P., Ciotti, L., & Sunyaev, R. A. 2005, MNRAS, 358, 168
Sazonov, S. Yu., Ostriker, J. P., & Sunyaev, R. 2004, MNRAS, 347, 144
Sazonov, S. Yu., Revnivtsev, M., Krivonos, R., Churazov, E., & Sunyaev, R. A. 2007, A&A, 462, 57
Sérsic, J. L. 1968, Atlas de Galaxias Australes (Cordoba: Obs. Astron.)
Silk, J., & Rees, M. J. 1998, A&A, 331, L1
Simoes Lopes, R. D., Storchi-Bergmann, T., de Fatima Saraiva, M., & Martini, P. 2007, ApJ, 655, 718
Soltan, A. 1982, MNRAS, 200, 115
Soria, R., Fabbiano, G., Graham, A. W., Baldi, A., Elvis, M., Jerjen, H., Pellegrini, S., & Siemiginowska, A. 2006, ApJ, 640, 126
Spergel, D. N., et al. 2007, ApJS, 170, 377
Springel, V., Di Matteo, T., & Hernquist, L. 2005, MNRAS, 361, 776
Tan, J. C., & Blackman, E. G. 2005, MNRAS, 362, 983
Thompson, T. A., Quataert, E., & Murray, N. 2005, ApJ, 630, 167
Thompson, T. A., Quataert, E., & Waxman, E. 2007, ApJ, 654, 219
Tremonti, C. A., Moustakas, J., & Diamond-Stanic, A. M. 2007, ApJ, 663, L77
Treu, T., Koopmans, L. V., Bolton, A. S., Burles, S., & Moustakas, L. A. 2006, ApJ, 640, 662
Weinberg, D. H., Hernquist, L., & Katz, N. 2002, ApJ, 571, 15
Wyithe, J. S. B., & Loeb, A. 2003, ApJ, 595, 614
Xu, H., et al. 2002, ApJ, 579, 600
Yan, R., et al. 2006, BAAS, 209, 181.05
Yu, Q., & Tremaine, S. 2002, MNRAS, 335, 965